AD NUMBER
AD380551
CLASSIFICATION CHANGES
TO: **UNCLASSIFIED**
FROM: **CONFIDENTIAL**
LIMITATION CHANGES
TO: **Approved for public release; distribution is unlimited.**
FROM: **Distribution authorized to U.S. Gov't. agencies and their contractors; Critical Technology; 21 APR 1967. Other requests shall be referred to U.S. Army Missile Command, Redstone Arsenal, AL 35809. This document contains export-controlled technical data.**
AUTHORITY
USAICOM ltr dtd 1 Feb 1974 USAICOM ltr dtd 1 Feb 1974

GENERAL
DECLASSIFICATION
SCHEDULE

IN ACCORDANCE WITH
DOD 5200.1-R & EXECUTIVE ORDER 11652

THIS DOCUMENT IS:

Subject to General Declassification Schedule of Executive Order 11652-Automatically Downgraded at 2 Years Intervals- DECLASSIFIED ON DECEMBER 31, 1972

BY

Defense Documentation Center
Defense Supply Agency
Cameron Station
Alexandria, Virginia 22314

CODE 25

SECURITY MARKING

The classified or limited status of this report applies to each page, unless otherwise marked.
Separate page printouts MUST be marked accordingly.

THIS DOCUMENT CONTAINS INFORMATION AFFECTING THE NATIONAL DEFENSE OF THE UNITED STATES WITHIN THE MEANING OF THE ESPIONAGE LAWS, TITLE 18, U.S.C., SECTIONS 793 AND 794. THE TRANSMISSION OR THE REVELATION OF ITS CONTENTS IN ANY MANNER TO AN UNAUTHORIZED PERSON IS PROHIBITED BY LAW.

NOTICE: When government or other drawings, specifications or other data are used for any purpose other than in connection with a definitely related government procurement operation, the U. S. Government thereby incurs no responsibility, nor any obligation whatsoever; and the fact that the Government may have formulated, furnished, or in any way supplied the said drawings, specifications, or other data is not to be regarded by implication or otherwise as in any manner licensing the holder or any other person or corporation, or conveying any rights or permission to manufacture, use or sell any patented invention that may in any way be related thereto.

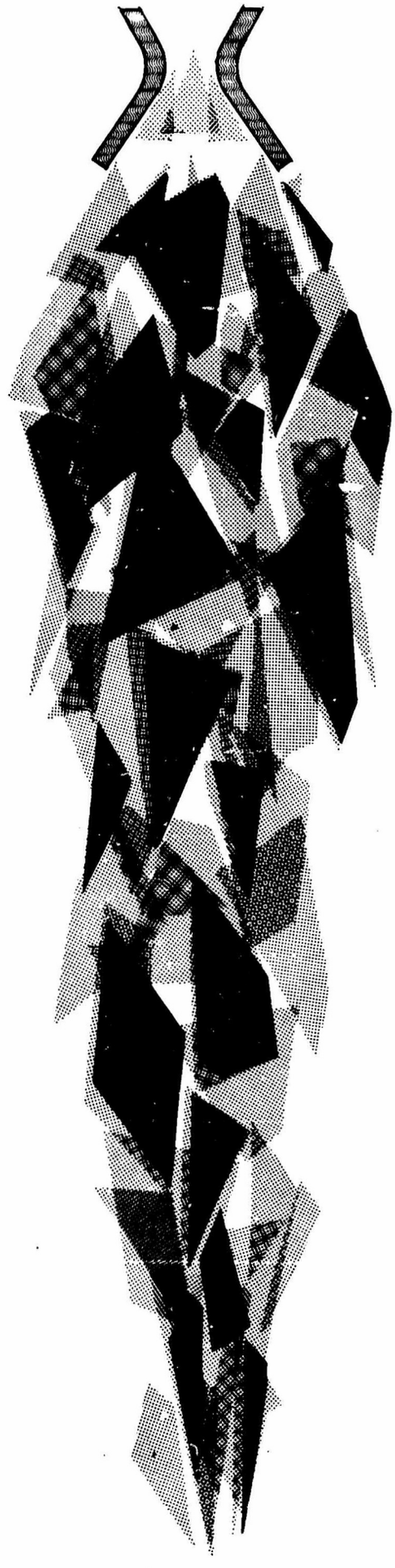

CONFIDENTIAL

COPY NUMBER [redacted]

REPORT NO. S-125

BALLISTIC SCALE-UP OF NF PROPELLANTS II. EVALUATION OF NF PROPELLANTS IN A 6-INCH MOTOR (INTERIM REPORT) (U)

U. S. ARMY MISSILE COMMAND

This document contains information affecting the national defense of the United States within the meaning of the Espionage Laws, Title 18, U.S.C., Sections 793 and 794. The transmission or the revelation of its contents in any manner to an unauthorized person is prohibited by law.

DOWNGRADED AT 3 YEAR INTERVALS:
DECLASSIFIED AFTER 12 YEARS.
DOD DIR 5200.10

ROHM AND HAAS
REDSTONE RESEARCH LABORATORIES
HUNTSVILLE, ALABAMA 35807

CONFIDENTIAL

CONFIDENTIAL

ROHM AND HAAS COMPANY

REDSTONE RESEARCH LABORATORIES
HUNTSVILLE, ALABAMA 35807

Report No. S-125

BALLISTIC SCALE-UP OF NF PROPELLANTS II. EVALUATION OF NF PROPELLANTS IN A 6-INCH MOTOR (INTERIM REPORT) (U)

by

Stanley E. Anderson

Approved by:

Louis Brown, Head
Ballistics Section

O. H. Loeffler
General Manager

Contributing Staff:

T. L. Cost

Publication date
April 21, 1967

(Work Completed
June 1966)

Contract No. DA-01-021 AMC-13864(Z)

CONFIDENTIAL

ROHM AND HAAS COMPANY

REDSTONE RESEARCH LABORATORIES
HUNTSVILLE, ALABAMA 35807

BALLISTIC SCALE-UP OF NF PROPELLANTS II. EVALUATION OF NF PROPELLANTS IN A 6-INCH MOTOR (INTERIM REPORT)(U)

ABSTRACT

Ballistic and mechanical properties of a representative NF propellant (RH-SE-103) are being evaluated in a 6-inch motor designed to have many of the characteristics required for a tactical application. A coned-cylindrical grain geometry was substituted for the original slotted-tube configuration on the basis of improved specific-impulse efficiency and low-temperature capability. The coned-cylindrical geometry was fired successfully at temperatures of -31° F, +77° F, and +135° F. The temperature coefficient was 0.13%/° F, exactly the same as had been measured in 2 × 4 motors. Specific impulse efficiency was 97% in both the 6CC18 and 6C5-11.4 motors.

Six-inch motors containing RH-P-112 were used to evaluate grain designs, to investigate the effect of grain design on specific-impulse efficiency, and to check analytical stress-strain predictions in low-temperature firings.

TABLE OF CONTENTS

ROHM AND HAAS COMPANY

REDSTONE RESEARCH LABORATORIES
HUNTSVILLE, ALABAMA 35807

BALLISTIC SCALE-UP OF NF PROPELLANTS II. EVALUATION OF NF PROPELLANTS IN A 6-INCH MOTOR (INTERIM REPORT)(U)

1. INTRODUCTION

Over the past several years, the formulation and scale-up of propellants based on NF binders has been a primary effort of these Laboratories. Extensive efforts in propellant research, development of processes for NF materials, and ballistic evaluation of the resulting propellants have been reported (1, 2, 3, 4, 5, 6, 7, 8).[1]

Although an 80-lbm test motor was fired for ballistic evaluation approximately one year ago (7), it was decided early in the program that further scale-up of propellant processing would be accompanied by the evaluation of the propellant in multiple smaller-scale motors rather than one large test motor. This would allow a more thorough investigation of reproducibility of specific impulse and burning rate, temperature coefficient, cycling capability, and storage life. To this end, a test motor having a diameter of 6 inches, a length of 18 inches, and a slotted-tube grain configuration was designed to approximate the characteristics required for a tactical application (9). The initial testing of this motor, designated 6ST18, has been discussed previously (6). These early ballistic results indicated a need for re-evaluation of the motor grain design. This report, the result of that study, discusses the analytical and experimental evaluations of the new coned-cylindrical design.

---

[1]Numbers in parenthesis identify references at the end of the report.

2. REVIEW OF 6ST18 DESIGN AND RESULTS

The 6 X 18 motor case was fabricated of mild-steel seamless tubing; the domed head closure contained a small opening to provide for mandrel alignment and for pressure measurements. The L/D ratio of the slotted-tube grain was 3 and the reduced web was 0.25. Motors were lined with NL-1 liner[1] and grains were cast by mandrel insertion. This motor was commonly referred to a. these Laboratories as the "Application Motor" (6); the grain and case design are illustrated in Fig. 1. In spite of the apparent simplicity of the design, two important disadvantages were found in early work.

Two firings of RH-SB-103cd[1] in the 6ST18 configuration gave an average specific impulse value of 257.9 lbf-sec/lbm which compared unfavorably with 262.8 lbf-sec/lbm measured in one 6C5-11.4 test motor. The same type of result was obtained in firings of RH-P-112 in the 6ST18. Calculations based on the specific impulse scaling techniques developed at these Laboratories (10) did not account for this discrepancy. For example, the predicted impulse of a 6ST18 with a plastisol nitrocellulose composite propellant RH-P-112cf[1] was 6.4 lbf-sec/lbm above that actually measured (Table I).

Table I

Specific Impulse Predictions for the Slotted Tube Using RH-P-112cf

	I_{sps} (lbf-sec/lbm)	
Motor	Predicted	Measured
6C5-11.4	--	244.8
6ST18	245.8	239.4

[1]Liner and propellant formulations are given in Appendix B.

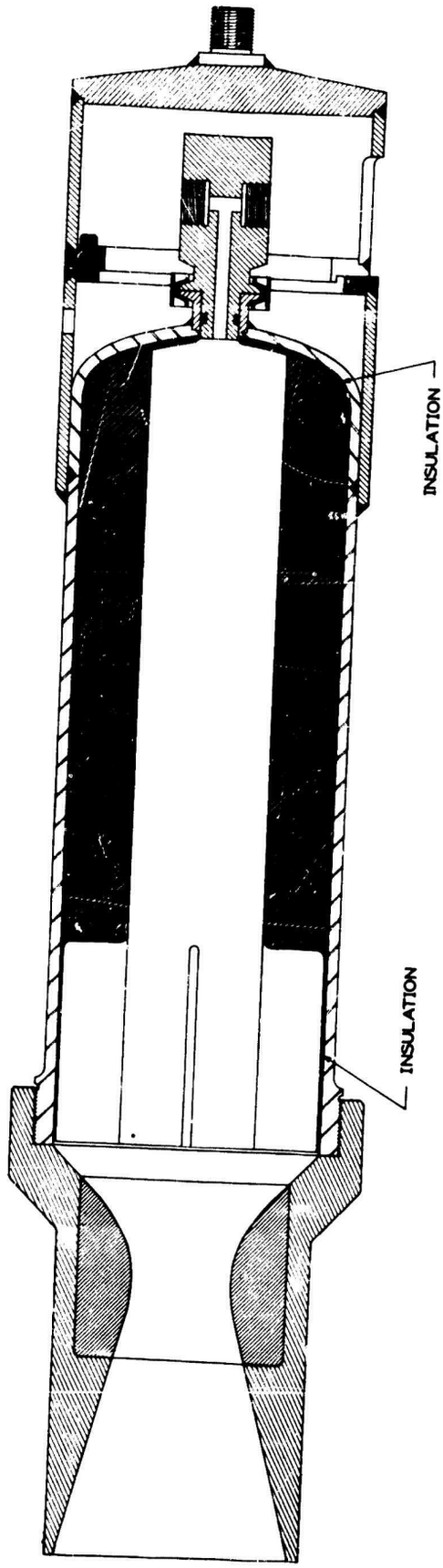

FIG. 1 APPLICATION MOTOR WITH SLOTTED-TUBE GRAIN.

The scaling procedure attempts to account for impulse losses due to two-phase flow effects and heat loss to the exposed case and nozzle area, and gives adequate specific impulse correlations for cylindrical geometries in which there is no localized high velocity flow on the chamber wall or nozzle. It was reasoned that the four slots in the ST configuration resulted in increased heat transfer (and lower impulse) because of the localized high velocity gas flow on the lined case, and that this situation is not treatable with the present scaling techniques.

In addition to the relatively poor specific impulse efficiency, an analysis (11) showed that undesirable strain magnifications were caused by the presence of the slots and the configuration of the head-end of the grain.[1] These magnifications could complicate failure predictions and data interpretation and detracted from the structural integrity of the motor. In view of these negative aspects of the slotted-tube design, efforts were directed toward obtaining a more attractive grain configuration which would give more representative specific impulse data and more useful strain and failure information.

3. DESIGN OF A CONED-CYLINDRICAL GRAIN

3.1 Preliminary Design

In a previous program, a cone was substituted for the slots in a slotted-tube grain without changing the pressure-time trace of the motor significantly (12). Small, but acceptable, reductions in propellant weight and thrust level did result from the change. In the Application Motor, the same sort of substitution was considered to eliminate the strain magnifications associated with the slots and to improve the flow conditions and specific impulse efficiency. Calculations showed that the most significant change in the grain would be a 6%

[1]Details are presented in Appendix C.

decrease in volumetric loading (Table II). The pressure-time trace from the coned-cylindrical grain (designated CC) would be the same as that from the 6ST18. The work in the following sections was done to see whether or not the anticipated benefits of the change would be realized.

Table II

Comparison of Parameters of Slotted-Tube (ST) and Coned-Cylindrical (CC) Grains

	ST	CC
Grain length, in.	18.0	18.0
Outside diameter of grain, in.	6.0	6.0
Inside diameter of grain, in.	3.0	3.0
Number of slots	4	N/A
Length of slots, in.	4.46	N/A
Length of cone, in.	N/A	4.5
Web, in.	1.5	1.5
Reduced web (w*)	0.25	0.25
Loading fraction	0.73	0.67

3.2 Specific-Impulse Evaluation with Plastisol-Nitrocellulose Propellants

In view of the relatively short supply and high cost of the NF raw materials, a complete study of the effects of grain design on specific impulse using NF propellant would not have been feasible. Therefore, these effects were evaluated using a well-characterized plastisol nitrocellulose composite propellant (designated RH-P-112cf). Specific impulse values were determined in firings of 6CC18, 6ST18, and 6C5-11.4 motors for comparison with each other and with predicted values. In this series of tests, the 6CC18 gave an efficiency close to that measured in the 6C5-11.4 and 1.4% higher than obtained in the 6ST18. Specific impulse predictions based on scaling techniques were still high for the 6CC18, indicating that unaccountable losses still existed (Table III).

Table III

Comparison of Specific Impulse Values for RH-P-112cf Measured in 6CC18, 6ST18, and 6C5-11.4 Motors

Motor Design	Number of Firings	Propellant Mass (lbm)	Predicted I_{sps} (lbf-sec/lbm)	I_{sps} (lbf-sec/lbm)	I_{sps}/I^0_{sps}
6ST18	3	20.38	245.8	239.4	0.926
6CC18	2	18.81	245.3	242.9	0.940
6C5-11.4	8	5.83	--	244.8	0.947

3.3 Analytical Structural-Integrity Comparison

The stresses and strains in the two grains were compared analytically at the same time that stress-relief methods for the head end were investigated (see Appendix C). Results of the calculations showed that the inclusion of a stress-relief fillet at the head end of the CC grain practically eliminated all strain magnifications (Table IV).

Table IV

Comparison of Strain Magnification Factors in ST and CC Grains

Location	Strain Magnification Factors	
	ST Grain	CC Grain
Aft end	4.0 (slots)	1.0
Center bore	1.0	1.0
Head end	3.1 (no fillet)	1.2 (with fillet)

3.4 Verification of Structural Integrity of 6CC18 Motors Containing RH-P-112cf

3.4.1 Problem Statement

Storage and firing temperature limits for the 6CC18 motor were defined by analytical studies of the effects of ignition loading, curing shrinkage, and thermal shrinkage on grain integrity. An additional area of concern was the very low strain capability of NL-1 liner, even at moderate temperatures. Experimental verification of the analysis using RH-P-112cf was desirable before tests of NF

propellants at temperature extremes were attempted. At the same time, the use of PL-33 (a brittle epoxy-based liner) in the plastisol motors would allow an assessment of the capabilities of such materials at low temperatures under firing conditions.

3.4.2 Analytical Results

The structural-integrity analysis for RH-P-112 grains[1] predicted adequate margins of safety for all storage and firing conditions except for very low temperatures. At -65°F both shrinkage and pressurization produced marginal conditions. For example, under pressurization loads the predicted strain was 0.45% while that available was 0.52% (Table V). These critical strains occurred in the head-end stress-relief fillet; failures would occur as circumferential cracks in this area.

Table V

Predicted and Allowable Stresses and Strains for Shrinkage and Pressurization Loadings in the 6CC18 and RH-P-112

Type of Loading	Temp. (°F)	Strain (%) Predicted/Allowable	Stress (psi) Predicted/Allowable
Shrinkage	-35	8.6/11.6	--
	-65	9.8/10.0	--
Pressurization	+135	0.52/11.8	6/62
	+78	0.52/11.6	8/87
	-35	0.50/5.4	120/781
	-65	0.45/0.52	321/2005

3.4.3 Experimental Results

Motors fired at +77°F were completely normal (Fig. 2), and a motor conditioned to -65°F showed no visible signs of failure upon inspection. However, the pressure-time history from a firing at -65°F indicated that additional surface opened up on ignition. The anomaly disappeared after 0.7 seconds and the remainder of the firing was

[1]Details are presented in Appendix E.

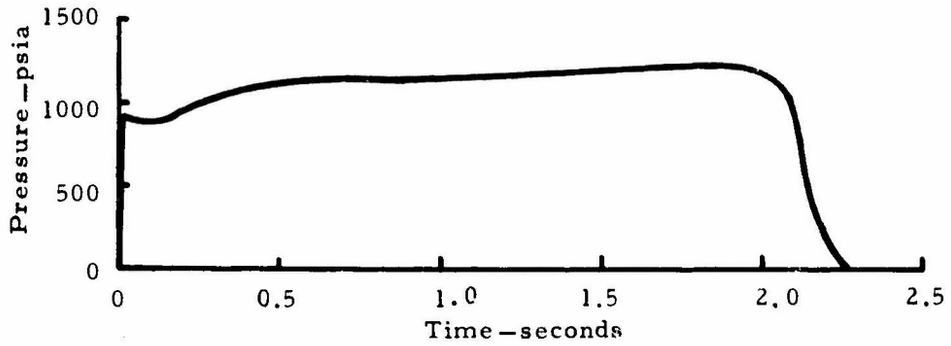

FIG. 2 PRESSURE-TIME RECORD FROM 6CC18 FIRING AT +77°F; RH-P-112cf PROPELLANT.

normal (Fig. 3). This behavior indicates that failure of the type predicted did occur, and that the results of the analysis were accurate. The brittle liner material did not cause any problem at -65°F.

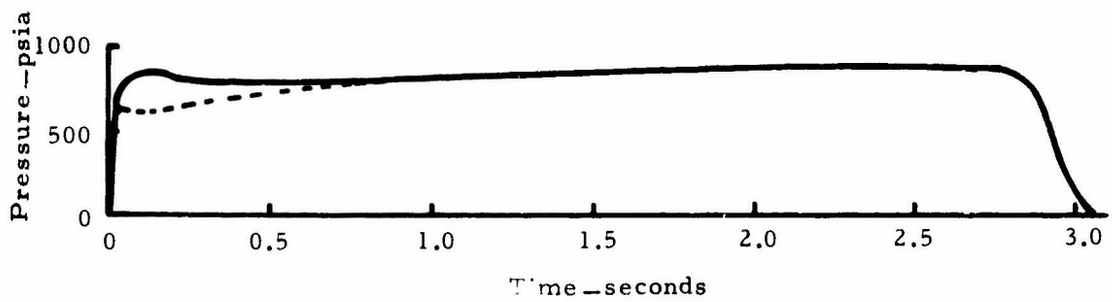

FIG. 3 COMPARISON OF PREDICTED PRESSURE-TIME RECORD (DOTTED LINE) WITH ACTUAL FIRING (SOLID LINE) AT -65°F, RH-P-112cf PROPELLANT.

3.5 Summary of Preliminary Investigations

The work reported above indicated that the preliminary coned-cylindrical grain design would give acceptable specific impulse data and that structural integrity should be improved over that of the slotted-tube. With the inclusion of a stress-relief fillet at the head-end, the design was accepted for the NF propellant evaluation program. The materials and production techniques used were the same as had been proven in the 6ST18 evaluation program. The final 6CC18 design is illustrated in Fig. 4.

4. PRELIMINARY EVALUATION OF NF PROPELLANT IN THE 6CC18 MOTOR

The analytical results for a 6CC18 containing RH-SE-103[1] propellant indicated a large margin of safety for storage at -65°F (a predicted strain of 8.5% but an available strain of 14.6%) but only a slight margin for firing at that temperature[2] (Table VI).

Table VI

Predicted and Allowable Stresses and Strains for Shrinkage and Pressurization Loadings in the 6CC18 with RH-SE-103

Type of Loading	Temp. (°F)	Strain (%) Predicted/Allowable	Stress (psi) Predicted/Allowable
Shrinkage	-35	7.4/20.0	--
	-65	8.5/14.6	--
Pressurization	+135	0.54/19.3	6/38
	+78	0.54/20.6	8/59
	-35	0.53/10.6	44/333
	-65	0.41/0.67	561/746

[1]Propellant formulations are presented in Appendix B.
[2]This analysis is presented in Appendix D.

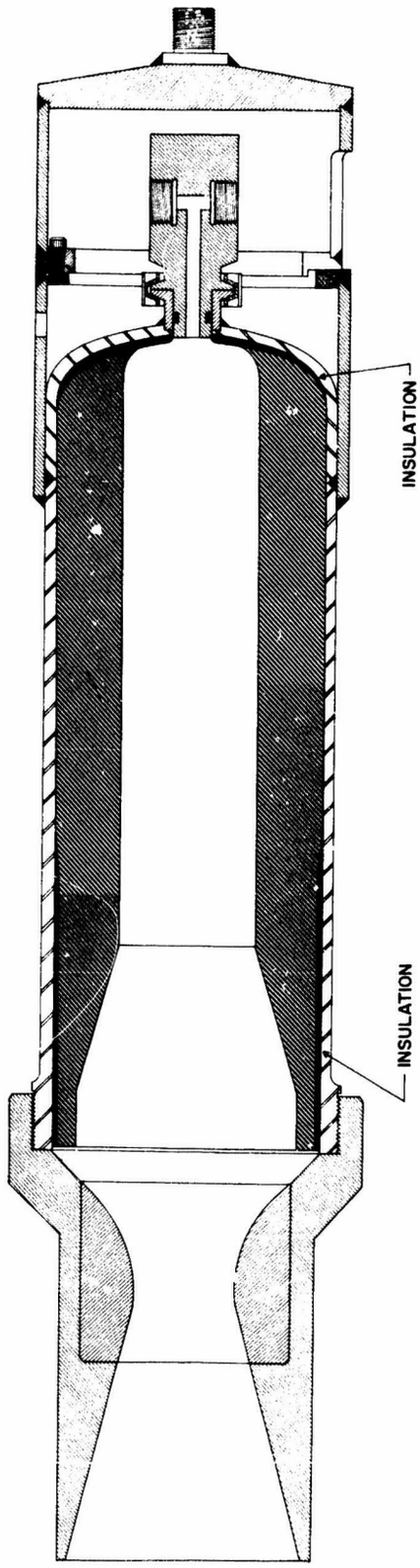

FIG. 4 APPLICATION MOTOR WITH CONED-CYLINDRICAL GRAIN.

Because of the marginal integrity at -65°F, no firings at that temperature were attempted. To assure that firings could be carried out at -35°F, a rapid hydrostatic pressurization system for testing an actual grain under simulated ignition conditions was developed.[1] Using the 6 × 18 motor, tests at -35°F showed that high rates of pressure rise could be obtained (Fig. 5). One 6CC18 was hydrotested at -35°F, and showed no failures. The same motor was later successfully fired at -31°F. Ballistic results from the test are discussed in Section 4.2.

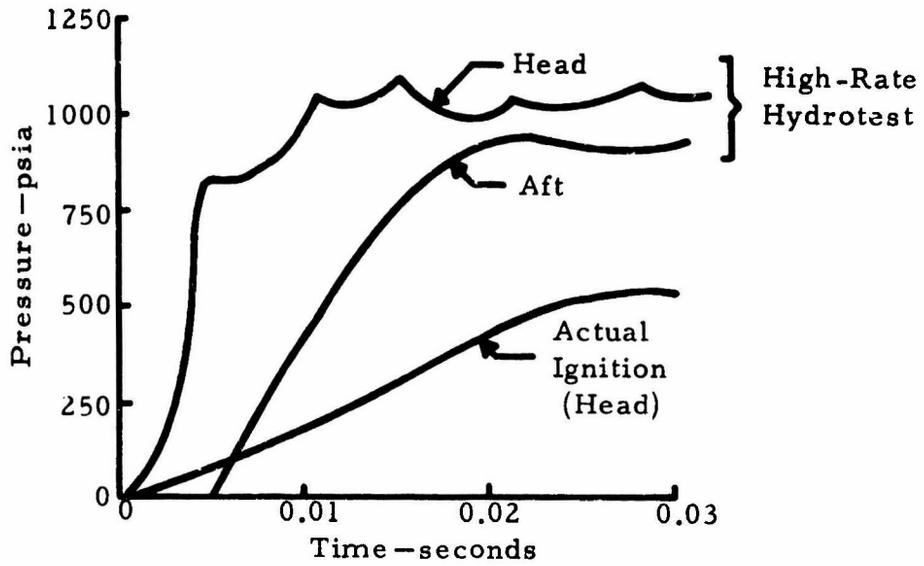

FIG. 5 COMPARISON OF HIGH-RATE HYDROSTATIC TEST WITH ACTUAL IGNITION OF 6CC18; BOTH TESTS AT ABOUT -30°F.

4.2 Ballistic Evaluation

Four 6CC18 motors were fired in this phase of the evaluation program. Two motors were cast from batch 1046 and fired successfully at +77°F for baseline data. Two 6CC18 motors and thirty 2C1.5-4.0 motors were cast from batch 1048. The small motors were used for batch check and also to determine the temperature coefficient

[1]The high-rate hydrotest system is discussed more fully in Appendix F.

for RH-SE-103. The large motors were fired at temperature extremes to check the small scale π_K determination. All tests were successful with specific impulse and pressure data being as expected (Table VII, Figs. 6 and 7). The specific impulse measured in the 6CC18 was very nearly equal to that from a 6C5-11.4 (Table VIII).

It should be noted that the SE- series propellants contain more inert ingredients (crosslinker) than did the SB- series, and SE-103af[1] burns about 10% slower than did SB-103cd; therefore, the specific impulse measured for RH-SE-103af is lower than that for RH-SB-103cd. This will explain the difference between the 6C5-11.4 value in Table VIII and that in Section 2.

Table VII

Ballistic Results from 6CC18 Motors

Round No.	K_n	T (°F)	$\bar{P}_b$ (psia)	$\bar{r}_b$ (in/sec)	$\bar{P}_a$ (psia)	Integral Ratio	I_{spd} (lbf-sec/lbm)	I_{sps} (lbf-sec/lbm)
6233	74.4	+77	957	1.22	937	0.98	250.5	259.1
6234	75.3	+77	935	1.18	916	0.98	251.7	260.2
6638	75.4	+135	955	1.20	924	0.97	254.1	259.8
6639	75.4	-31	765	0.97	702	0.97	244.9	255.9

Table VIII

Comparison of Specific Impulse Values from 6CC18 and 6C5-11.4

Motor	No. Fired	I_{sps} (lbf-sec/lbm)
6CC18	2	259.7
6C5-11.4	2	260.0

[1]The af subscript designates a 55μ mean oxidizer particle size coated with 1% Alon-C.

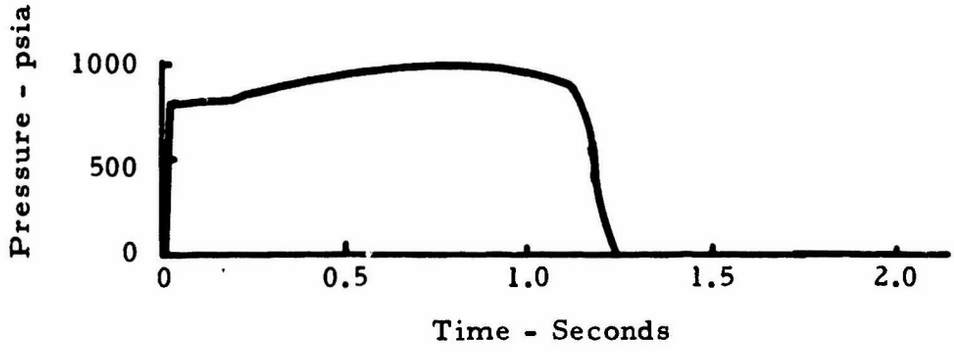

FIG. 6 PRESSURE-TIME RECORD FROM 6CC18 FIRING AT +77°F; RH-SE-103af PROPELLANT, BATCH 1046.

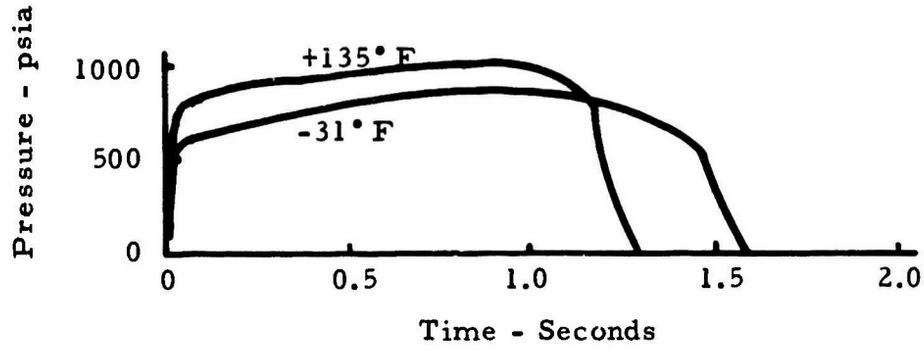

FIG. 7 PRESSURE-TIME RECORDS FROM 6CC18 FIRINGS AT TEMPERATURE EXTREMES; RH-SE-103af PROPELLANT, BATCH 1048.

The agreement between π_K data from the large motors and the small batch-check motors was excellent (Fig. 8).

5. RESULTS AND EXTENSIONS

Several important results have been obtained from this preliminary work. No significant obstacles to tactical use of this propellant have been found. An adequate interim liner material has been demonstrated in four motors with RH-SE-103.

Scale-up of the NF propellant process to 50-lbm batches and larger from which two 20-lbm motors were cast proceeded smoothly,

and burning rates and temperature coefficients in the large motor were essentially identical with those measured in 2 × 4 motors. The coned-cylindrical grain gave better specific-impulse efficiency than did the slotted tube.

The superiority of the coned-cylindrical grain over the slotted-tube design with respect to strain requirements has also been demonstrated. The stress analysis techniques applied to the NF motors were verified in tests with plastisol composite propellant.

Extensions are planned to better demonstrate extreme-environment capability. One motor is currently being cycled between -35°F and +135°F, and has completed 3 cycles with no signs of degradation. Other motor tests planned include additional cycling tests, high and low temperature storage, and high and low temperature firing.

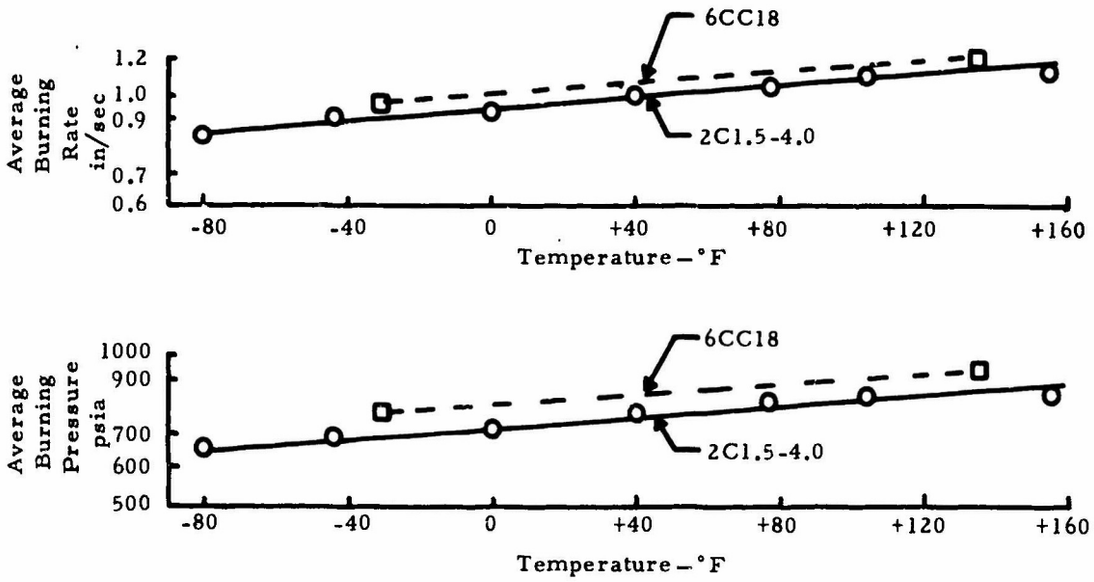

FIG. 8 COMPARISON OF TEMPERATURE COEFFICIENT DATA FROM 6CC18 WITH THAT FROM 2C1.5-4.0 BATCH-CHECK MOTORS.

REFERENCES

1. Baldwin, M. G. and Foster, J. S., "NFPA-TVOPA Propellants," Bulletin of the 21st Interagency Solid Propulsion Meeting, p. 283, July 1965.

2. Staff of Rohm and Haas Redstone Research Laboratories, "Scale-Up of High Energy Propellants," Bulletin of the ICRPB/AIAA Solid Propulsion Conference, Vol. I, p. 33, July 1966.

3. Nipp, B. K., "Process Development of a Binder Consisting of NFPA Copolymer and the Plasticizer, TVOPA, "Rohm and Haas Company Report S-107, October 1966.

4. Chaille, J. L., "Scale-Up of NF Prepolymer Propellant Processing-I," Rohm and Haas Company Report S-97, September 1966.

5. Parrott, J. W., "Production of NF Chemicals for Advanced Research Projects Agency," Rohm and Haas Company Report S-110, September 1966.

6. Anderson, S. E. and Thompson, B. L., "Ballistic Characteristics of NF Propellants," Rohm and Haas Company Report S-85, October 1965.

7. Anderson, S. E. et al., "Ballistic Scale-Up of NF Propellants I. 80-lbm Motor Demonstration Firing," Rohm and Haas Company Report S-94, March 1966.

8. Pratt, T. H., "The Explosive Characteristics of NF Compounds and Propellants," Rohm and Haas Company Report S-79, October 1965.

9. Anderson, S.E., "Application of NF Propellants – A Study Report," Rohm and Haas Company Report S -62, May 1965.

10. Cockrell, B. L., "Ballistic Evaluation of Propellants in Micro-Motors," Rohm and Haas Company Report S-49, October 1964.

11. Becker, Eric B. and Brisbane, John J., "Application of the Finite Element Method to Stress Analysis of Solid Propellant Rocket Grains Vol. I", Rohm and Haas Company Report S-76, November 1965.

12. Rohm and Haas Company Report S-31, "Final Report on Missile A Booster Development," July 1961.

APPENDIX A

Glossary

1. List of Acronyms

AA	Acrylic acid
Al	Aluminum
AP	Ammonium perchlorate
HMDI	Hexamethylene di-isocyanate
HPMA	Hydroxypropyl methacrylate
NFPA	2, 3-bis(difluoramino)propyl acrylate
TVOPA	1, 2, 3-tris[α, β-bis(difluoramino)ethoxy]propane
P	Designation for propellants based on nitrocellulose/ TEGDN binder.
SB	Designation for binder based on a copolymer of NFPA and HPMA, crosslinked with HMDI.
SE	Designation for binder based on a copolymer of NFPA and AA, crosslinked with a diepoxide.

2. List of Symbols

I_{spd}	Measured (delivered) propellant specific impulse, lbf-sec/lbm.
I_{sps}	Standard deliverable propellant specific impulse, lbf-sec/lbm.
I^0_{sps}	Standard theoretical propellant specific impulse, lbf-sec/lbm.
Integral Ratio	- Ratio of burning pressure integral to total pressure integral.
K_n	Burning surface to throat area ratio
$\overline{P}_a$	Action time average chamber pressure, psia
$\overline{P}_b$	Burning time average chamber pressure, psia
$\overline{r}_b$	Average regression rate, in/sec
T	Temperature, °F
ϵ	Expansion Ratio
w*	Web thickness of propellant/outside diameter of grain.

APPENDIX B

Propellant and Liner Formulations

1. Propellants

Ingredient	Wt. % SB-103cd	SE-103af	P-112cf
NFPA/HPMA prepolymer	13	--	--
NFPA/AA prepolymer	--	13	--
TVOPA	26	26	--
Double-base powder	--	--	16.7
TEGDN	--	--	37.3
AP (35μ) 1% TCP	46	--	--
AP (55μ) 1% TCP	--	--	34
AP (55μ) 1% Alon-C	--	46	--
Al (Alcoa 140)	15	15	15
Resorcinol	--	--	1
HMDI crosslinker (added)	~0.4	--	--
Epoxide crosslinker (added)	--	~2.0	--

2. Liners

Ingredient	Wt. % NL-1	PL-33
Paraplex® [a] P-13	35.0	--
Paraplex P-43	35.0	--
Hysol 2039 [b]	--	20.4
Hysol 3579	--	26.6
Asbestos [c] (7TF-1)	30.0	20.0
Cellulose Acetate	--	8.0
TEGDN	--	23.0
Lupersol DDM® [d] (added)	1.0	--
DMP® [a]-10	--	2.0

[a] Rohm and Haas Company, Philadelphia, Pennsylvania.
[b] Hysol Corporation, Olean, New York.
[c] Johns-Manville, New York, New York.
[d] Wallace & Tiernan Inc., Newark, New Jersey.

APPENDIX C

Comparison of the Maximum Shrinkage Strains in Two Application Motor Grain Designs

Work done by: T. L. Cost

INTRODUCTION AND SUMMARY

A comparative study was made of the maximum strains produced by shrinkage in two grain designs suitable for use in the advanced propellant application motor. The grains were similar in that they both had hollow circular cylindrical shapes with an inside diameter of 3 in., an outside diameter of 6 in., and a length of 18 in. However, the grains differed in the configuration of the aft end. One grain (the 6CC18) had a cone-shaped aft end (Fig. C-1) while the other grain (the 6ST18) had a slotted aft end (Fig. C-2). No particular propellant mechanical behavior was assumed in the analysis and only shrinkage loads were considered. Results of the study indicated the grain with the cone-shaped aft end (6CC18) was superior from a structural-integrity standpoint to the grain with the slotted aft end (6ST18). The maximum strains in the head ends of both motors were found to be equal and relatively large. Hence, two methods for modifying the design and thereby reducing the strains in the head end were studied. It was found that the addition of a fillet at the head-end termination of the grain-case interface reduced the strain such that the strains in the head end were only approximately 1.17 times as high as the strains in an equivalent infinite-length cylinder.

DETAILS OF ANALYSIS

The finite element method was used whenever possible in analyzing the strains in the two grains. Existing computer programs used at these Laboratories are limited to the analysis of either three-dimensional axisymmetric bodies or two-dimensional (plane stress or plane strain) bodies. Much more approximate estimates must be made to account for other geometries. Since only a comparative study was made of the two grains, the actual material properties used in the analysis were immaterial. However, they are included here for

completeness. A Young's modulus of 10,800 psi and a Poisson's ratio of 0.497 (K = 600,000 psi) were used in calculating the strains. All results were obtained for a linear thermal shrinkage of -0.00767 in/in which corresponds to a temperature change of -100°F for a material with a volumetric expansion coefficient of 0.023%/°F. A rigid case was assumed in analyzing both geometries.

1. Analysis of 6CC18 Grain

The 6CC18 grain is a completely axisymmetric body (Fig. C-1) and can be analyzed directly by the finite element method. The stresses, strains, and displacements were determined for the thermal shrinkage and material properties described above and the results are presented in Figs. C-3—C-5. Fig. C-3 illustrates the deformed and undeformed shape of the 6CC18 grain. The actual displacements of the boundary of the 6CC18 motor grain have been magnified 5 times the actual size and plotted to the scale shown in Fig. C-3 for easier interpretation. Figs. C-4 and C-5 contain maximum stress and maximum strain contours plotted on the profile of the grain. As indicated in Figs. C-4 and C-5, strain concentrations exist at the forward termination of the case-grain interface, point A. The magnitude of the strain at point A was determined to be 8.6%. The strain at the aft end of the motor occurred at point B, Fig. C-5, and was determined to be approximately 2.0%. In the middle of the grain at the inner bore, point C, Fig. C-5, the maximum strain (circumferential) was determined to be 2.8%.

Since the magnitudes of the shrinkage stresses depend almost directly on the value of Young's modulus, the magnitudes of the stresses in Fig. C-4 are immaterial and are only included to give an indication of the stress distribution. Presumably, solid propellant materials experience a stress relaxation effect which makes the stresses of little consequence in thermal shrinkage problems with low cooling rates, provided the temperature of interest is not too far below the transition temperature of the propellant.

2. Analysis of 6ST18 Grain

By inspection of Fig. C-2, the 6ST18 grain (Fig. C-2) is seen to be a general three-dimensional body and is too complex to be analyzed by existing finite element method programs at these Laboratories. Consequently, approximations must be made to the actual geometry in order to perform an analysis. As a first approximation, the slots were ignored in the 6ST18 motor. This approximation resulted in an axisymmetric body which was analyzed by the finite element method. The stresses and strains were similar to those in the 6CC18 motor everywhere except at the aft end. The strain in the axisymmetric body at the aft end of the grain-case interface was found to be approximately 6%. In the actual 6ST18 slotted-end grain, strains on the order of 6% would likely occur at the aft end of the grain-case interface halfway between each pair of slots. To account for the slots, a strain magnification factor of 4 was estimated to occur at the forward end of the slots. When applied to the strains calculated by the finite element method at the point where the base of the slot occurs, the maximum strain in the vicinity of the forward end of the slots was estimated to be 11.1%.

DISCUSSION OF RESULTS

The maximum strains in the 6CC18 and 6ST18 motors at various critical points are summarized in Fig. C-6. Inspection of this figure gives an indication as to the relative merit of each design from a structural integrity standpoint. The slots in the 6ST18 motor result in much higher strains than in the 6CC18 cone-shaped aft end motor. Apparently, the 6CC18 is the better of the two designs.

Although the strains in the aft end of the 6CC18 motor are small, the strains in the head-end are large enough to be of concern. The ratio of the strain in the head end to the strain in the middle of the grain at the inner bore is 8.6/2.8 or 3.07. Thermal shrinkage strains at moderately low temperatures would very likely be large enough, due to the 3.07 concentration factor, to produce failure. Hence, means for reducing the magnitude of the concentration factor were studied.

Two methods for reducing the strains at the head end were investigated. The first method involved releasing the grain from the case at the grain-case interface for a certain distance. This concept, commonly referred to as a "booted" grain, is illustrated in Fig. C-7a. The second method involved the addition of a stress-relief fillet at the forward of the grain-case interface. This concept is illustrated in Fig. C-7b. Both of the geometries in Fig. C-7 were analyzed by the finite element method.

The displacement, maximum normal stress contours, and maximum normal strain contours are shown in Figs. C-8 – C-10, respectively. As is apparent, the point where the maximum stress and strain occurs has shifted from point A in Fig. C-9 to point B. However, the maximum strain at point B is approximately 5.0%. This magnitude of strain represents a strain concentration factor of 5.0/2.8 or 1.79 according to the definition above.

The stresses and strains in the 6CC18 with the stress-relief fillet added, as indicated in Fig. C-7b, were determined and found to be equal to the stresses and strains in the 6CC18 grain without the radius except near the head end. The maximum strain at the head end with the fillet was determined to be 3.3%. This magnitude represents a strain concentration factor as described above of only 3.3/2.8 or 1.17.

CONCLUSIONS

From the results of the study described, several conclusions can be drawn concerning the effectiveness of the various grains from a structural integrity standpoint.

1. The maximum strains in the aft end of the 6CC18 motor were 2.0% while those in the aft end of the 6ST18 motor were 11.1%. Thus, the 6CC18 motor is the better of the two designs.

2. The maximum strains in the head end of the 6CC18 and 6ST18 motor were both 8.6% which represented a strain concentration factor of 3.07. This concentration factor is large enough to warrant modification of the 6CC18 grain near the head end.

3. The concept involving releasing the head end from the case results in a maximum strain of 5.0% and a strain concentration factor of 1.79.

4. The concept of adding a stress-relief fillet at the head end resulted in a strain of 3.3% and a strain concentration factor of 1.17. Thus, the stress-relief fillet is the better of the two stress relief methods investigated.

5. The strain concentration factor of 1.17 very nearly represents the lowest concentration factor possible. With the stress-relief fillet included in the 6CC18 design, the strain conditions at the head end of the motor should only be slightly more severe than the strain conditions at the middle of the motor at the inner bore.

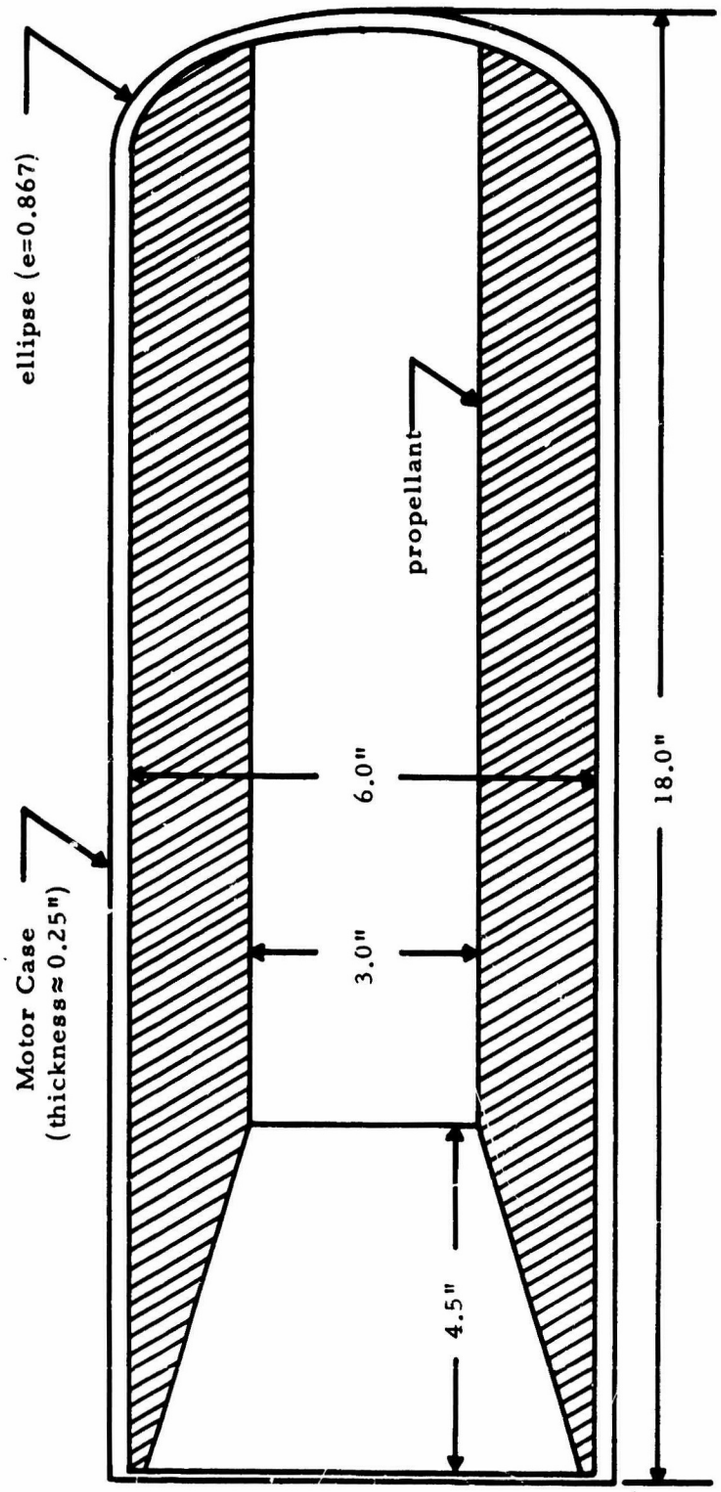

FIG. C-1 CROSS-SECTION OF 6CC18 APPLICATION MOTOR; NO STRESS-RELIEF FILLET.

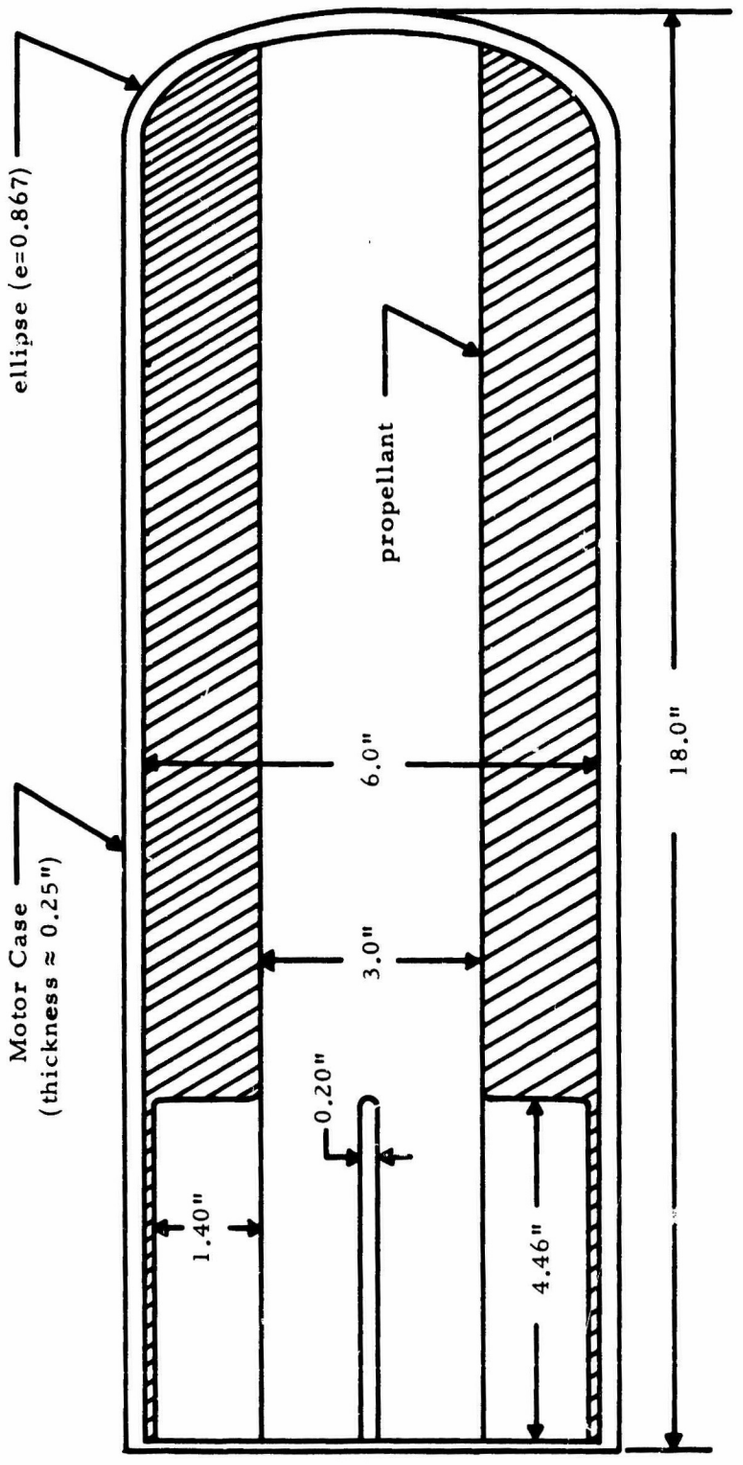

FIG. C-2 CROSS-SECTION OF 6ST18 APPLICATION MOTOR.

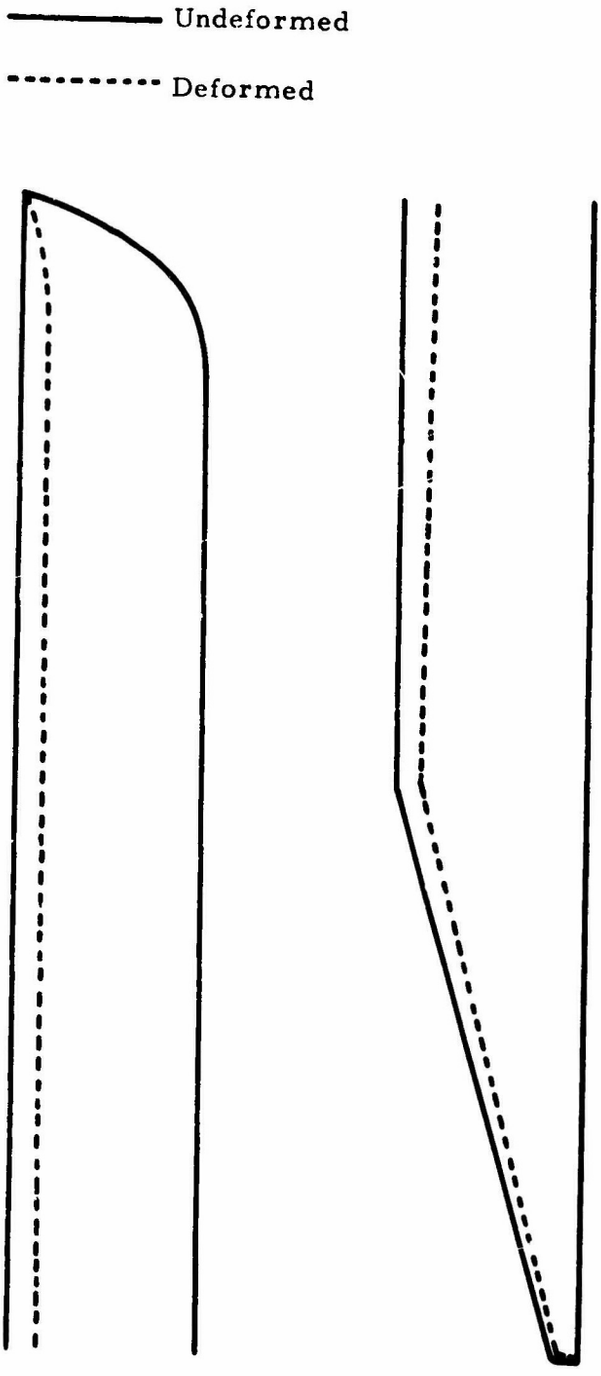

FIG. C-3 DEFORMED AND UNDEFORMED PROFILES OF 6CC18 APPLICATION MOTOR GRAIN UNDER THERMAL SHRINKAGE LOADING ($\alpha \Delta T$ =-0.00767 in/in).

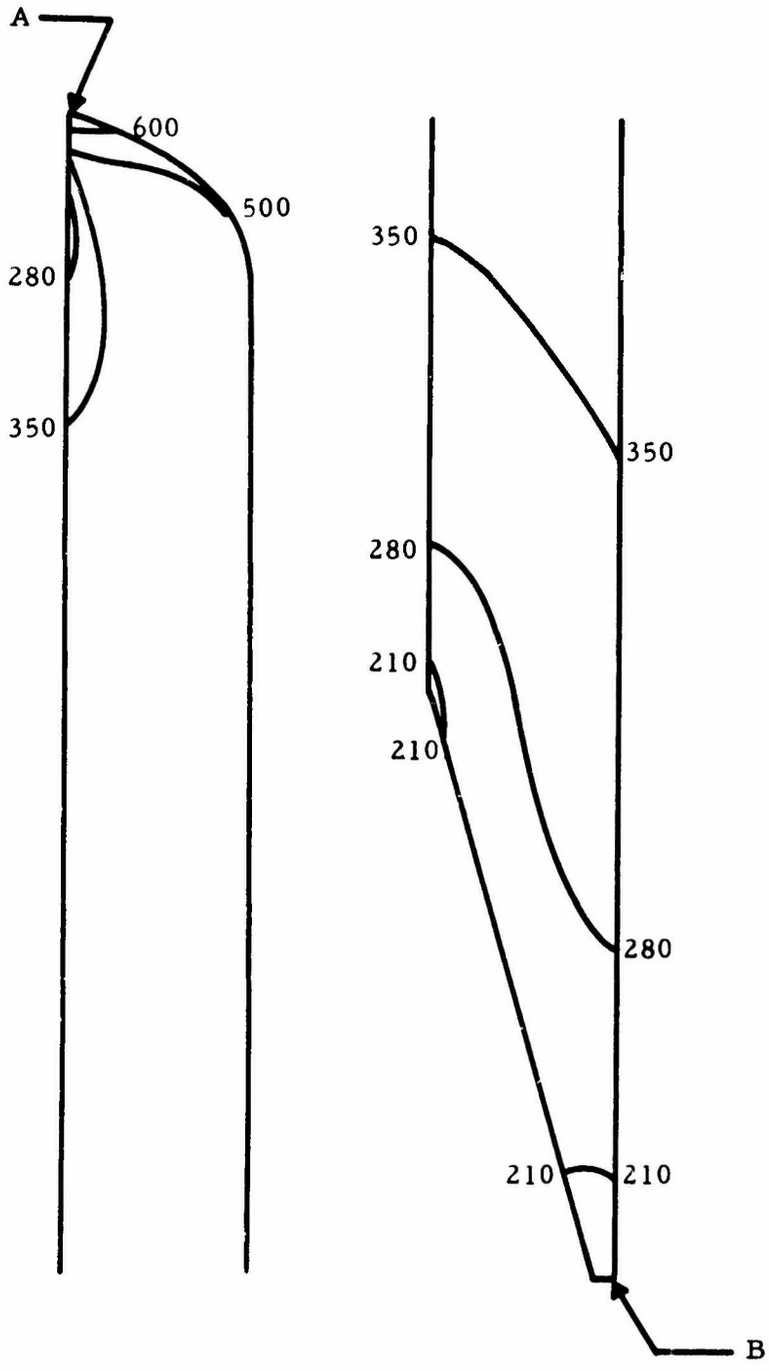

FIG. C-4 MAXIMUM STRESS CONTOURS (psi) FOR 6CC18 GRAIN UNDER THERMAL SHRINKAGE LOADING ($\alpha\Delta T$ = -0.00767 in/in).

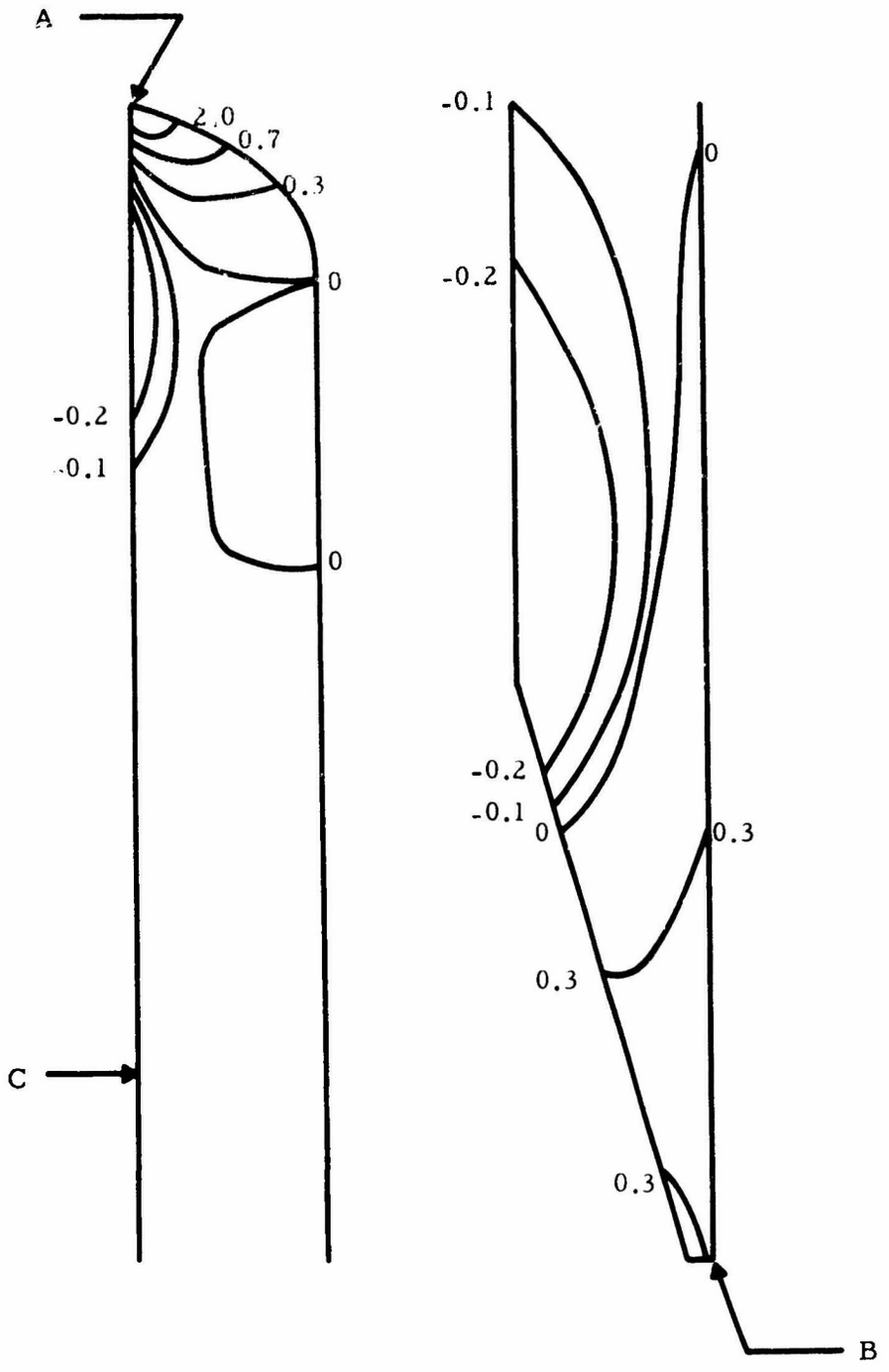

FIG. C-5 MAXIMUM NORMAL STRAIN CONTOURS (%) FOR 6CC18 GRAIN UNDER THERMAL SHRINKAGE LOADING ($\alpha\Delta T$ = -0.00767 in/in).

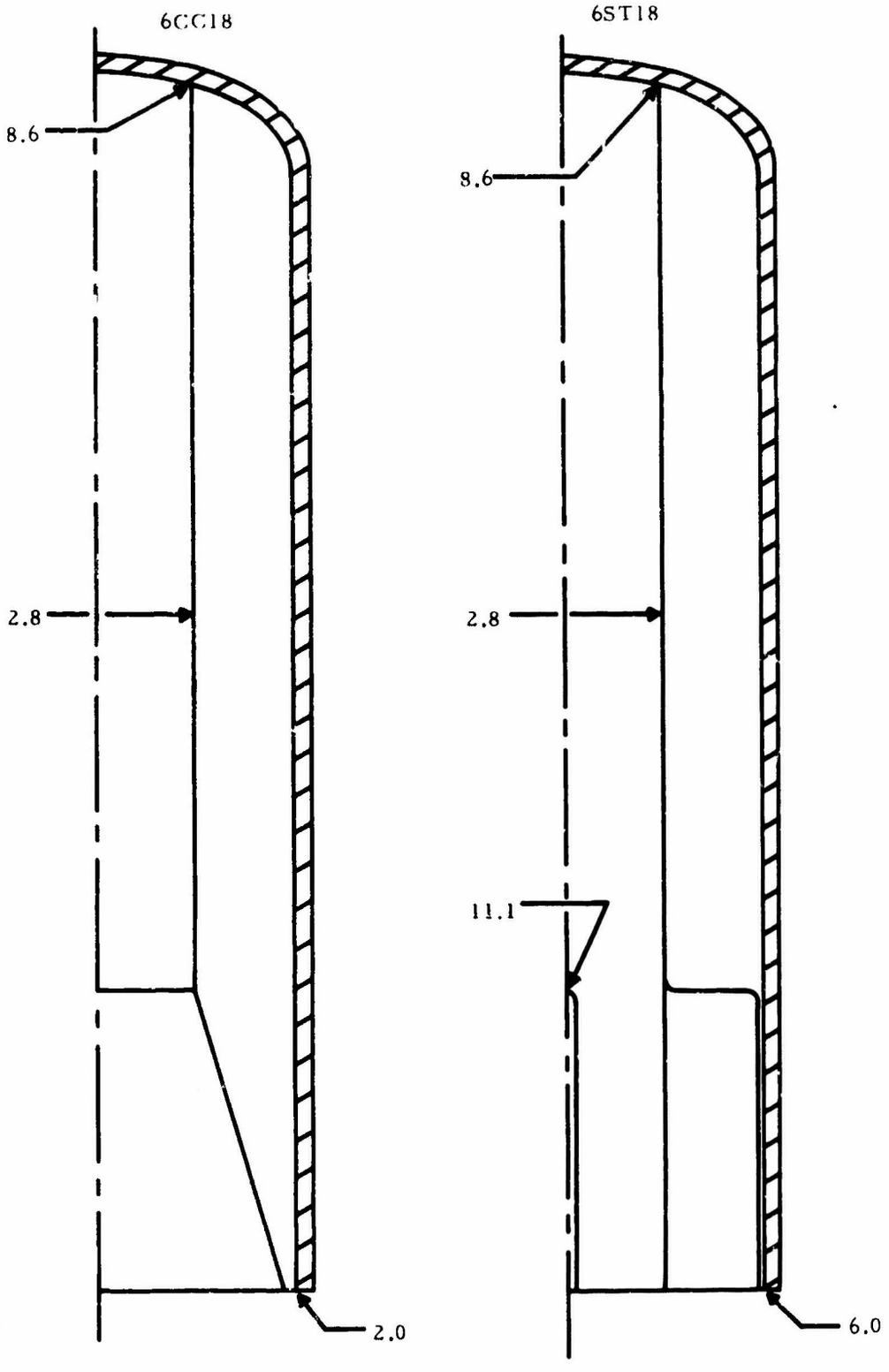

FIG. C-6 SUMMARY OF MAXIMUM STRAINS (%) IN CRITICAL AREAS OF 6CC18 AND 6ST18 APPLICATION MOTORS UNDER THERMAL SHRINKAGE LOADING.

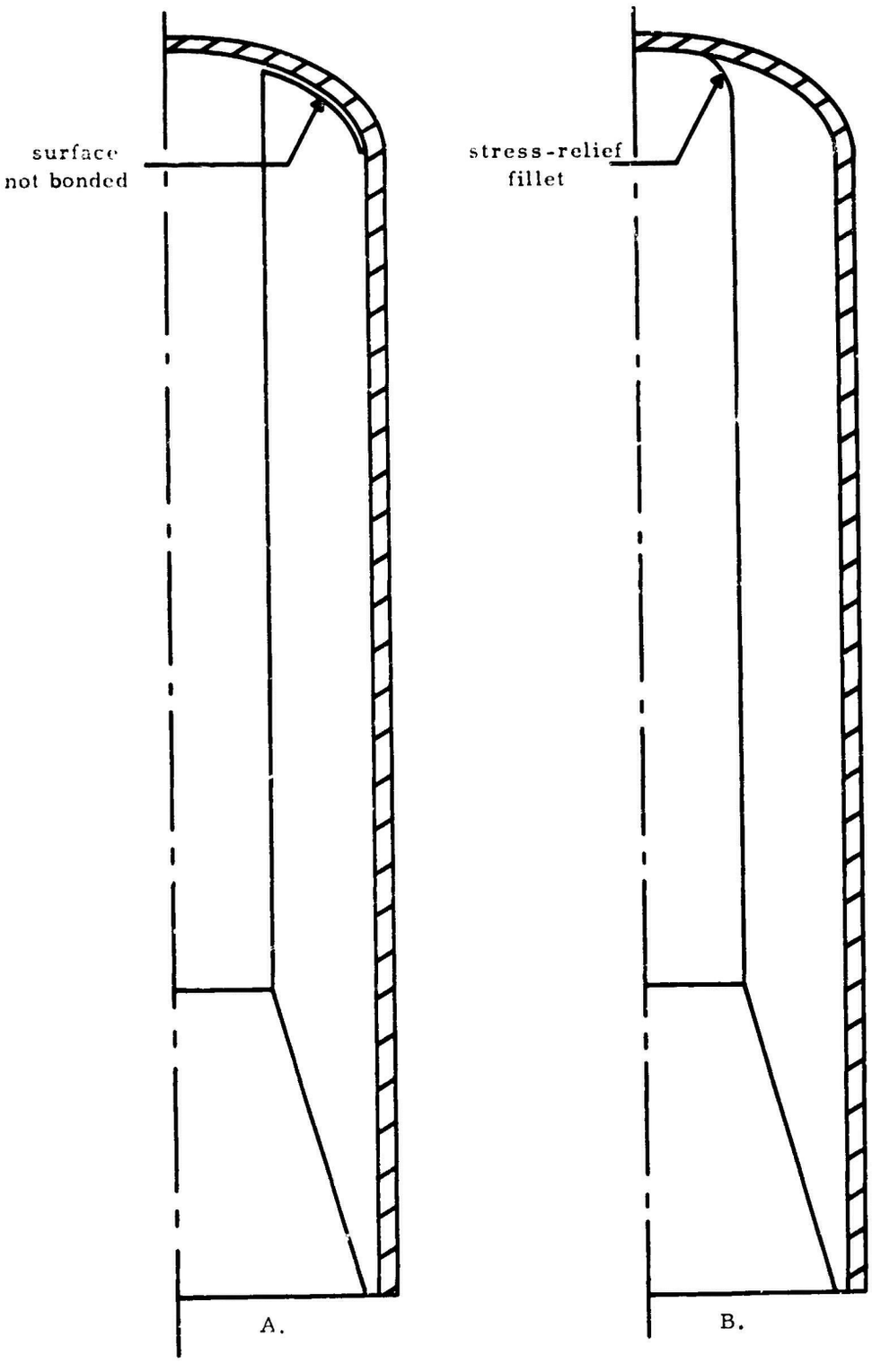

FIG. C-7 TWO HEAD-END CONFIGURATIONS FOR RELIEVING STRAINS IN APPLICATION MOTOR DUE TO THERMAL SHRINKAGE LOADING.

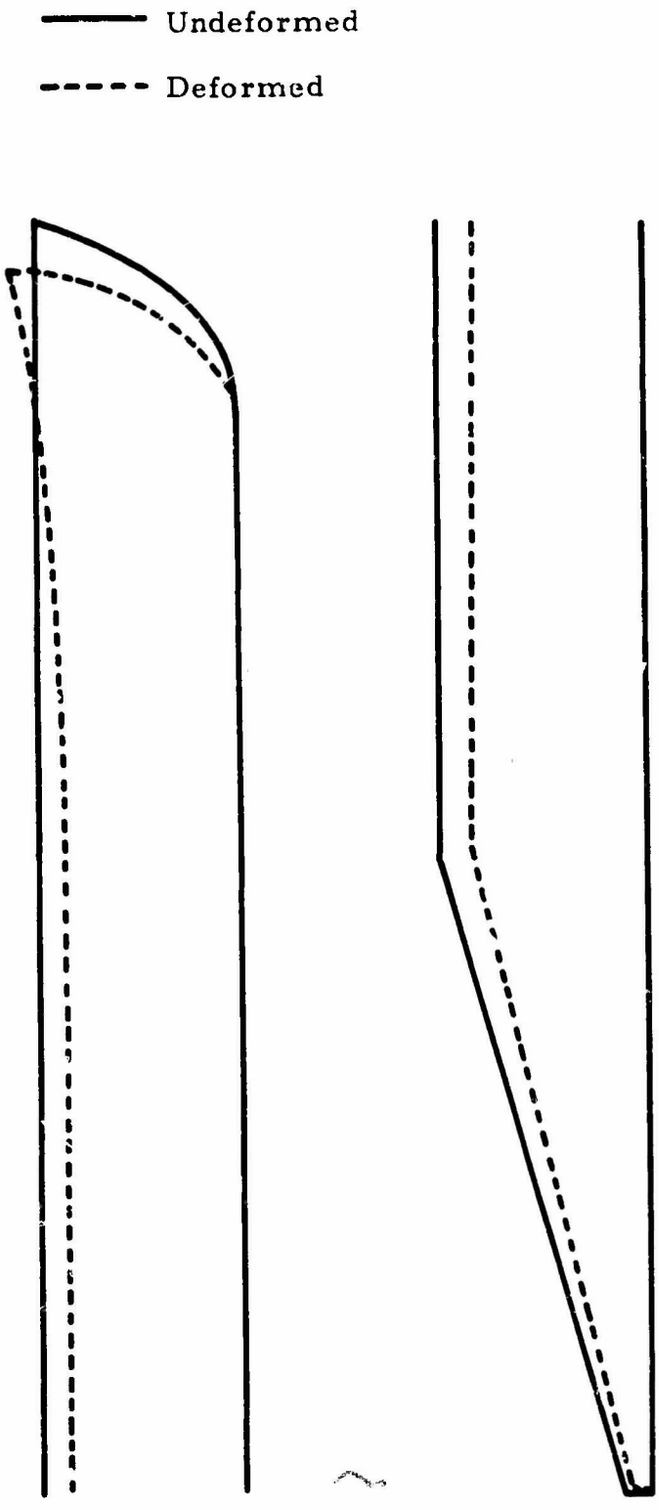

Fig. C-8 DEFORMED AND UNDEFORMED PROFILES OF BOOTED 6CC18 GRAIN UNDER THERMAL SHRINKAGE LOADING ($\alpha\Delta T$ = -0.00767 in/in).

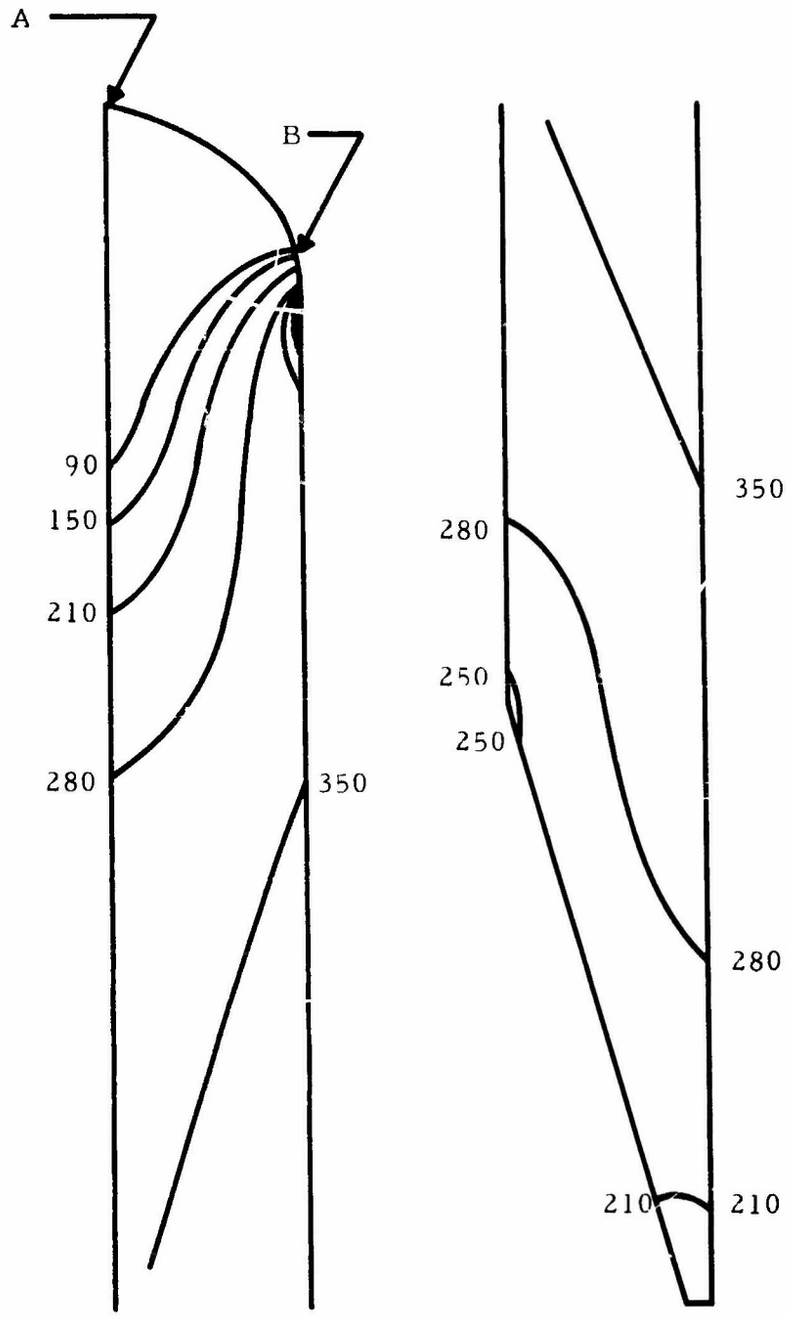

FIG. C-9 MAXIMUM NORMAL STRESS CONTOURS (psi) FOR BOOTED 6CC18 GRAIN UNDER THERMAL SHRINKAGE LOADING ($\alpha\Delta T$ = -0.00767 in/in).

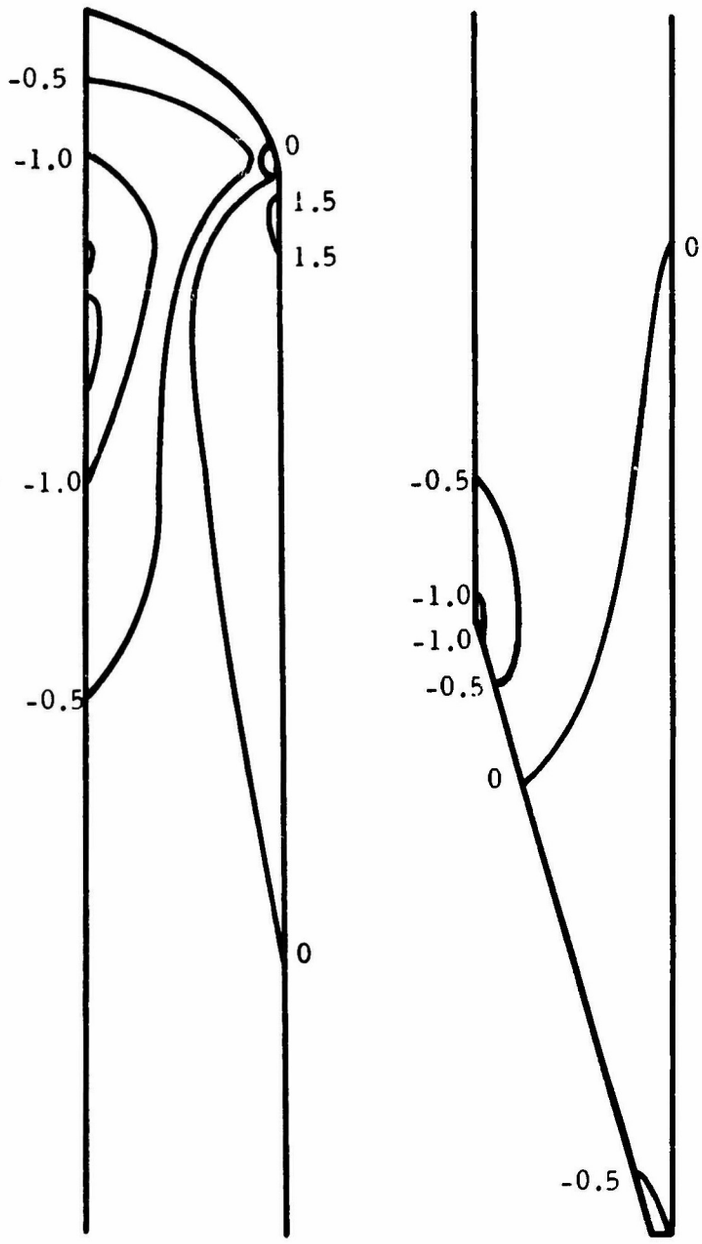

FIG. C-10 MAXIMUM NORMAL STRAIN CONTOURS (%) FOR BOOTED 6CC18 GRAIN UNDER THERMAL SHRINKAGE LOADING ($\alpha\Delta T$ = -0.00767 in/in).

APPENDIX D

Structural Integrity of the Advanced Propellant Application Motor Containing RH-SE-103 Propellant

Work done by: T. L. Cost

INTRODUCTION AND SUMMARY

A determination of the structural integrity of the advanced propellant application motor (6CC18) was made utilizing a propellant designated SE-103A.[1] The loading conditions investigated were shrinkage resulting from curing at +140°F and cooling to -35°F and -65°F, and pressurization resulting from ignition at +135°F, +78°F, -35°F, and -65°F. The experimental data currently available do not adequately define the mechanical behavior at low temperatures (-65°F) and high rates (30 in/in/min); however, estimates were made for these conditions. From the data now available, it appears that SE-103 in the 6CC18 will perform satisfactorily under all conditions examined except pressurization at -65°F.

STRUCTURAL INTEGRITY ANALYSIS

The configuration of the advanced propellant application motor analyzed is the 6CC18 design which is a completely axisymmetric body with a cross section as shown in Fig. D-1. The finite element method for elastic, axisymmetric bodies was used in performing the analysis. The conditions examined included shrinkage from +140°F to -35°F and -65°F and pressurization at +135°F, 78°F, -35°F and -65°F. The chamber pressure upon ignition was assumed to increase to a constant value of 1000 psia in 10 msec.

1. Mechanical Properties

From tests of SE-103 in uniaxial tension, the mechanical properties (modulus, maximum stress, strain at maximum stress, and the shift factor) illustrated in Figs. D-2, D-3, D-4, and D-5 have been obtained.

[1] Mechanical properties on which this analysis was based were obtained from batch SE-103A-1039.

The propellant was assumed to be perfectly elastic in dilation and a bulk modulus of 350,000 psi was assumed. The volumetric coefficient of thermal expansion β was determined from several strain evaluation cylinders (SEC's[1]) to be 0.02%/°F. The case was assumed to be of static test hardware and constructed of mild steel with a Young's modulus of 30×10^6 and a Poisson's ratio of 0.3. The case thickness was assumed to be 0.25 in.

From Fig. D-5 the shift factor for SE-103 was determined for the four temperatures of interest as indicated previously. The results are presented in Table D-I.

Table D-I

SE-103 Shift Factors as a Function of Temperature

Temp. (°F)	$\log_{10}(a_T)$
+135	-1.9
+78	0
-35	7.9
-65	11.6

2. Strain Rates

In general, the rate of loading of solid propellant materials influences both the predicted and allowable stresses and strains; hence, reasonable estimates must be made of this quantity.

a. Shrinkage - Preliminary calculations based upon a volumetric thermal expansion coefficient β of 0.02%/°F indicated that the application motor would experience a change in maximum normal strain of 0.03%/°F. Cooling the motor from room temperature (78°F) to -65°F would result in a temperature change of 143°F and hence an applied strain of 4.25%. To be conservative, a strain of 5% was assumed applied in a cooldown time of 500 min. The strain rate resulting from this assumption is

[1]The SEC's used to determine β contained SE-103-1023 propellant.

$$\dot{\epsilon}_s = \frac{0.05 \text{ in/in}}{500 \text{ min.}} = 10^{-4} \frac{\text{in/in}}{\text{min}}$$

This strain rate was assumed in analyzing the cooldown to -35°F.also.

b. Pressurization - The measured pressure-time curve for an application motor similar to that shown in Fig. D-1 but without the fillet present at the head end of the motor is shown in Fig. D-6. As indicated in the figure, the time needed to reach maximum pressure is 10 msec. If the total amount of strain is assumed to be applied in this length of time, the strain rate is

$$\dot{\epsilon}_p = \frac{0.005}{0.01} \frac{\text{in/in}}{\text{sec}} \cdot \frac{60 \text{ sec}}{\text{min}} = 30 \frac{\text{in/in}}{\text{min}}$$

This calculation is based upon a preliminary calculatior which indicated that strains upon pressurization would not be greater than 0.5%.

3. Reduced Times

For the strain rates assumed in Section 2 and the shift factors presented in Table I, the reduced times of interest for the shrinkage and pressurization analyses are presented in Table D-II. With these reduced times, the appropriate physical properties can be obtained from Figs. D-2—D-4.

Table D-II

Reduced Times

Temp. (°F)	Shrinkage $\log \frac{1}{\dot{\epsilon}_s a_T}$ (95/5)	Pressurization $\log \frac{1}{\dot{\epsilon}_p a_T}$ (95/5)
+135		+0.42
78		-1.48
-35	-3.90	-9.38
-165	-7.60	-13.08

4. Predicted Stresses and Strains

The finite element method was used to predict the stresses and strains in the application motor. The stress analysis was begun before the modulus values of the propellants were available and, hence, for the pressure loading, the stresses and strains were obtained for a range of modulus values.

a. Shrinkage - The propellants were assumed to cure at +140°F and to experience a cure shrinkage which resulted in a tensile strain of 1%. Calculations indicated that the maximum normal strain would occur approximately at Point A in Fig. D-1. The magnitude of this predicted strain is 0.03%/°F. In addition, for failure predictions, the thermal shrinkage term $(\beta/3)$ should be added to the actual strain. From these data, the predicted values for the strain at -35°F and -65°F are shown in Table D-III.

Table D-III

Predicted Shrinkage Strains

	-35°F	-65°F
Strain due to cure shrinkage	= 1%	= 1%
Strain due to thermal shrinkage load	(0.03)(175) = 5.25%	(0.03)(205) = 6.15%
Strain due to thermal shrinkage	(0.00667)(175) = 1.17%	(0.00667)(205) = 1.37%
Total strain from unstressed state	7.42%	8.52%

Note that the shrinkage strains are not dependent upon the modulus for this motor.

b. Pressurization - To determine the stresses and strains resulting from pressurization at the temperatures of interest, the modulus of the propellant must be determined from Fig. D-2 for the reduced times of interest as presented in Table D-II. The modulus values are shown in Table D-IV.

Table D-IV

Tangent Modulus for SE-103

Temp. (°F)	E (psi)
+135	204
78	316
-35	4160
-65	66000

As mentioned previously, for the pressurization problem the stresses and strains were determined for a range of modulus values. The maximum stress, which occurs approximately at point A (see Fig. D-1) in the application motor, is shown as a function of modulus in Fig. D-7. Also shown in Fig. D-7 is the maximum normal strain (hoop) in the cylindrical portion of the grain (point B, Fig. D-1). The strain at point B was found to be equal to the strain in an infinitely long cylinder of the same outside diameter and web fraction as the application motor. From D-7 an indication can be obtained of the stress magnification in the head end of the motor (point A) as compared with the strain away from the ends of the motor (point B). A similar plot of the maximum strain as a function of modulus is shown in Fig. D-8. From these figures, the predicted stresses and strains can be determined which correspond to the modulus values in Table D-IV. These predicted values are presented in Table D-V..

Table D-V

Predicted Stresses and Strains for Pressurization[a]

Temp. (°F)	Stress (psi)	Strain (%)
+135	6	0.542
78	8	0.542
-35	44	0.534
-65	561	0.407

[a]The stress values in Table D-V ignore the 1000 psi hydrostatic pressure.

5. Allowable Stresses and Strains

At these Laboratories the uniaxial tensile test is the only test performed to determine the failure characteristics of solid propellants at moderate to high rates. Since the stress field in a solid propellant grain is multiaxial, the uniaxial data are not directly applicable although the uniaxial data can be modified with a great deal of approximation to account for multiaxial effects. The maximum allowable stresses and strains for the uniaxial case can be determined from Figs. D-3 and D-4. The allowable values are determined for the reduced times shown in Table D-II and the results are presented in Tables D-VI and D-VII.

Table D-VI

Allowable Uniaxial Strains for Shrinkage Loading

Temp. (°F)	ϵ (%)
-35	30
-65	22

Table D-VII

Allowable Uniaxial Stresses and Strains for Pressurization Loading

Temp. (°F)	σ (psi)	ϵ (%)
+135	48	29
78	74	31
-35	417	16
-65	932	1

6. Discussion of Results

As mentioned in Section 5, the uniaxial failure data obtained at these Laboratories is not directly applicable to the multiaxial stress fields present in the actual motor. Multiaxial tests which more closely simulate the actual service loads are performed by some propellant manufacturers and, hence, some knowledge is available of the effect of multiaxial stress fields on stresses and strains at failure.

From the data available, it appears that the failure strains in a biaxial stress field can be as small as 67% of the failure strains in a uniaxial field. In regard to the multiaxial effect upon failure stresses, the situation is not as well defined. This can be illustrated by considering the failure envelopes of several popular failure theories in terms of a biaxial stress condition as shown in Fig. D-9. It can be seen that for some theories the effect is to strengthen the material while for other theories the effect is to weaken the material. To be conservative the maximum allowable tensile stresses for multiaxial conditions will be taken as 80% of the allowable uniaxial tensile stresses to account for the multiaxial effects.

If the above assumptions are used to modify the allowable stresses and strains shown in Tables D-6 and D-7, comparisons can be made of the predicted and allowable stresses and strains. These comparisons are shown in Tables D-VIII and D-IX.

Table D-VIII

Comparison of Predicted and Allowable Strains for Shrinkage Loading

Temp. (°F)	Strain[a] (%)/(%)
-35	7.42/20
-65	8.52/14.6

[a] Predicted/allowable

It should be kept in mind that the allowable stress values in Table D-IX were also obtained from uniaxial tests at atmospheric pressure whereas the predicted stresses have a hydrostatic pressure of 1000 psi superimposed over the values presented. Also, the pressurization results presented in Table D-IX do not account for the damage which has been done to the propellant by shrinking to the temperatures

shown or of other thermal cycling damage. This damage cannot adequately be accounted for with the data available.

Table D-IX

Comparison of Predicted and Allowable Stresses and Strains for Pressurization Loading

Temp. (°F)	Stress[a] (psi)/(psi)	Strain[a] (%)/(%)
+135	6/38.4	0.542/19.3
+78	8/59.1	0.542/20.6
-35	44/333.0	0.534/10.6
-65	561/746.0	0.407/0.670

[a] Predicted/allowable

It should be kept in mind that this analysis is based upon a very thick case. For flight-weight hardware and particularly for fiberglas motor cases, the pressurization results could be influenced considerably. Also, the effects of ablation have not been accounted for. Since the surface burns away, the original grain configuration most likely would never experience the maximum chamber pressure although a different (burned) geometry will.

7. Conclusions

Keeping in mind the limitations of the analysis as discussed in the previous sections, several conclusions can be drawn concerning the results of the analysis.

a. SE-103 should withstand storage at all temperatures from -65°F to +135°F.

b. SE-103 should withstand firing at all temperatures from -35°F to +135°F, but is marginal at -65°F.

c. As indicated in Figs. D-7 and D-8, the stresses and strains at the head end of the application motor are not significantly greater than those in the cylindrical portion of the grain where conditions closely resemble an infinite length cylinder. Thus, only a very small concentration factor exists.

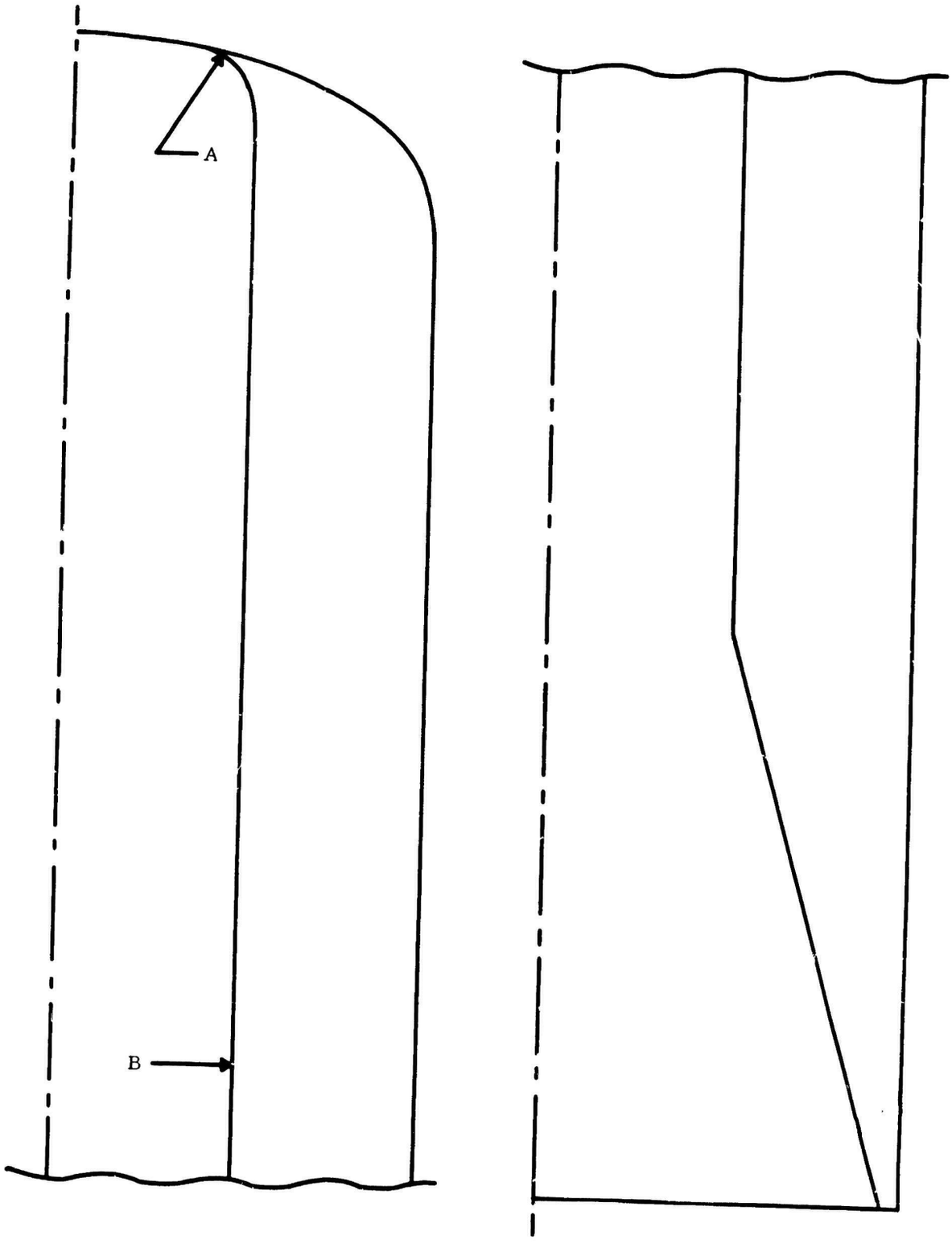

FIG. D-1 CROSS-SECTION OF 6CC18 APPLICATION MOTOR GRAIN WITH STRESS-RELIEF FILLET; LENGTH = 18 in., O.D. = 6 in., I.D. = 3 in.

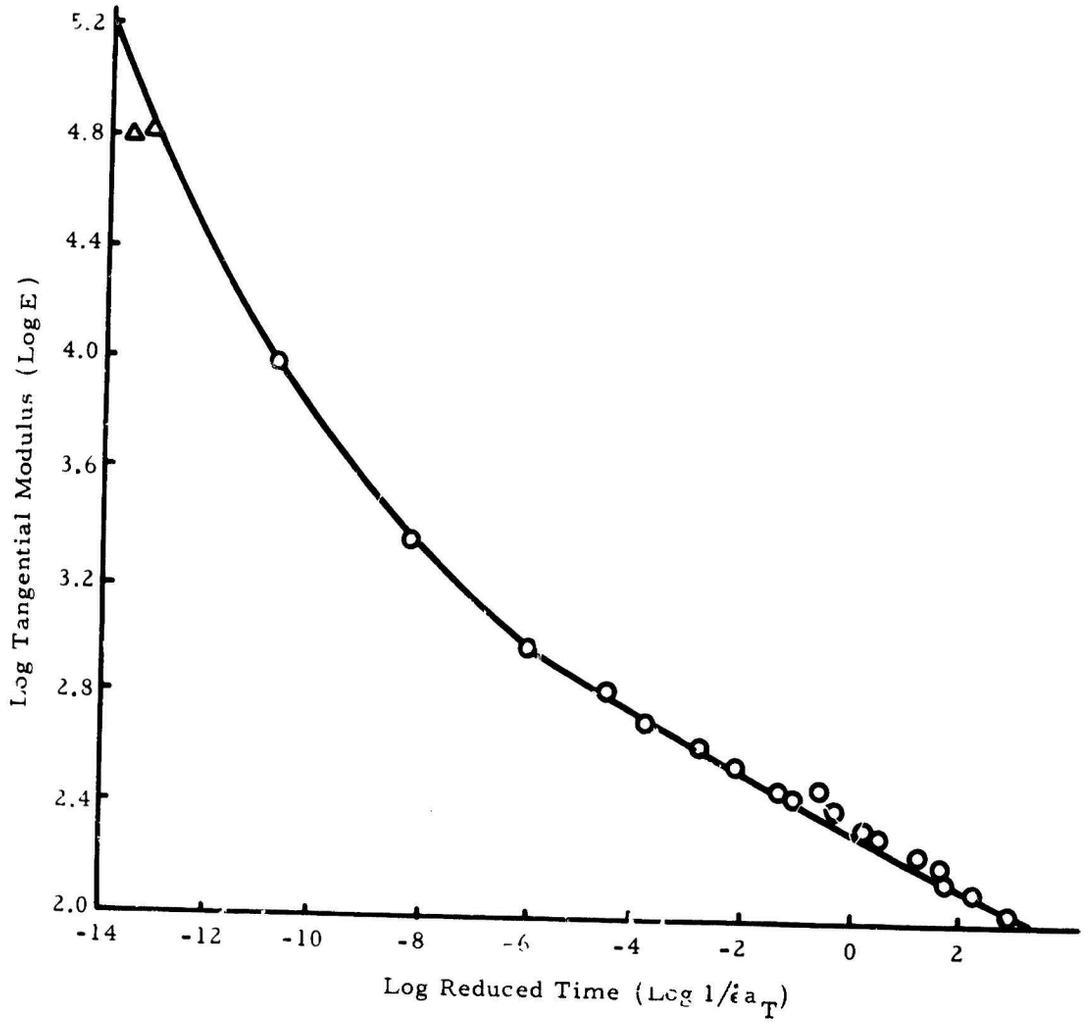

FIG. D-2 TANGENT MODULUS VERSUS REDUCED TIME FOR RH-SE-103 PROPELLANT.

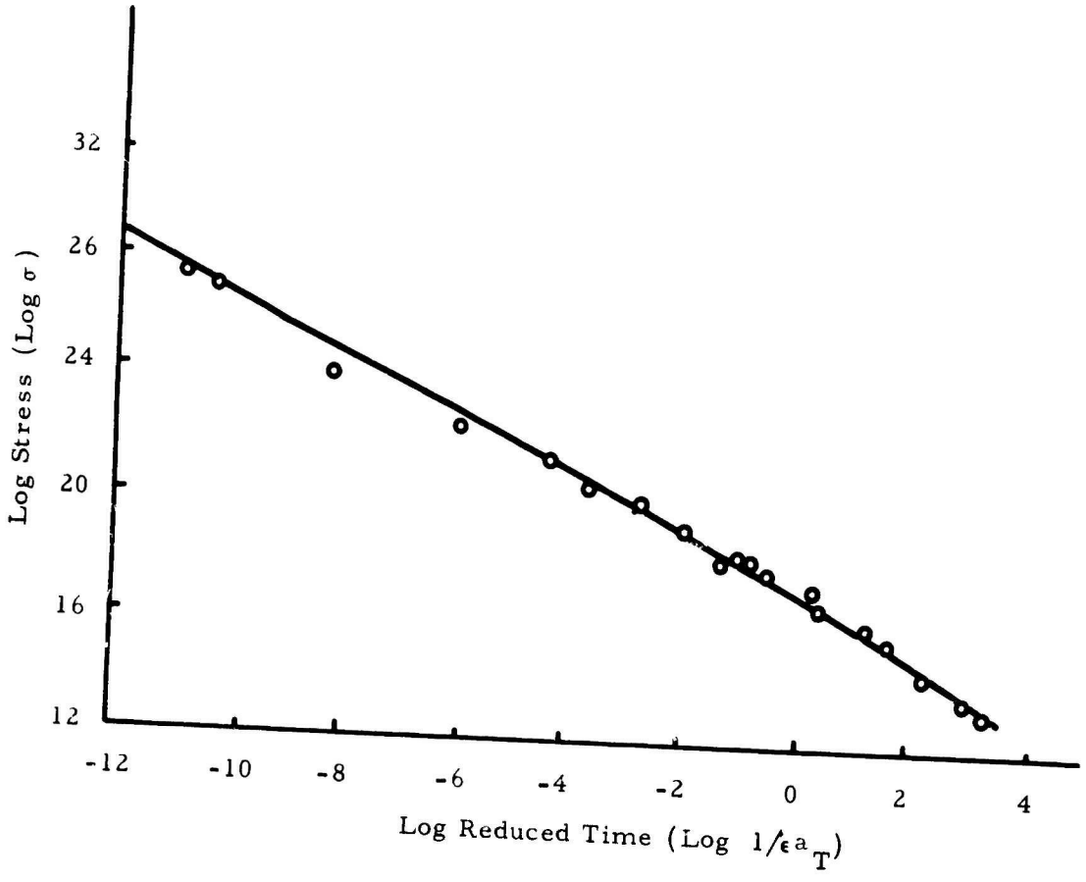

FIG. D-3 MAXIMUM STRESS VERSUS REDUCED TIME FOR RH-SE-103 PROPELLANT.

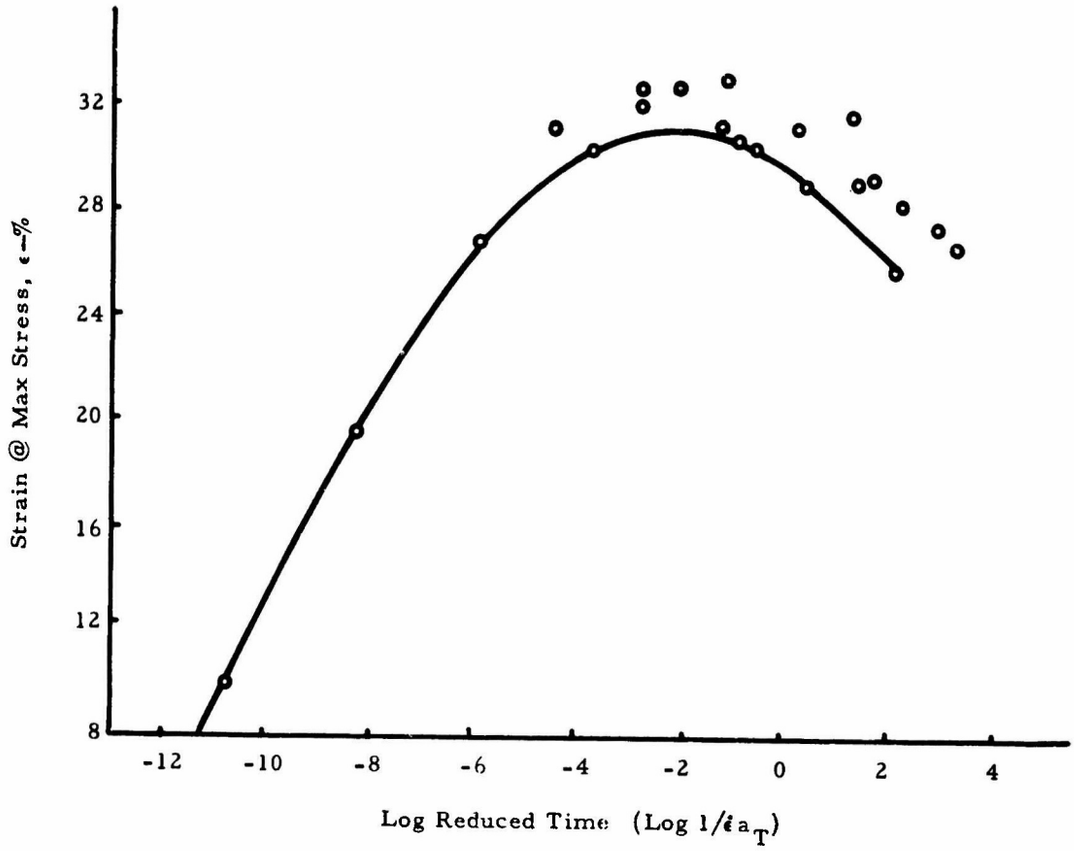

FIG. D-4 STRAIN AT MAXIMUM STRESS VERSUS REDUCED TIME FOR RH-SE-103 PROPELLANT.

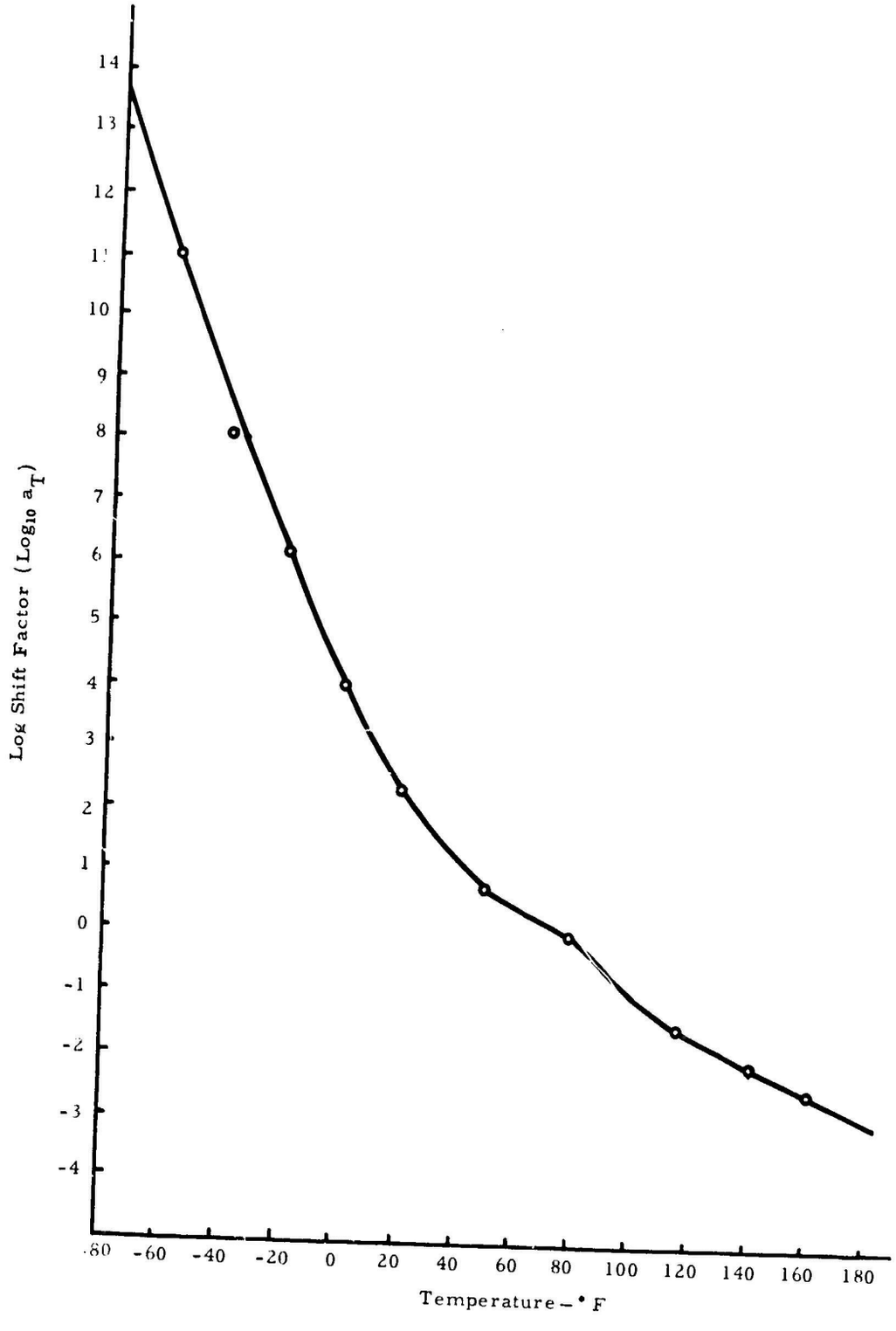

FIG. D-5 SHIFT FACTOR VERSUS TEMPERATURE FOR RH-SE-103 PROPELLANT.

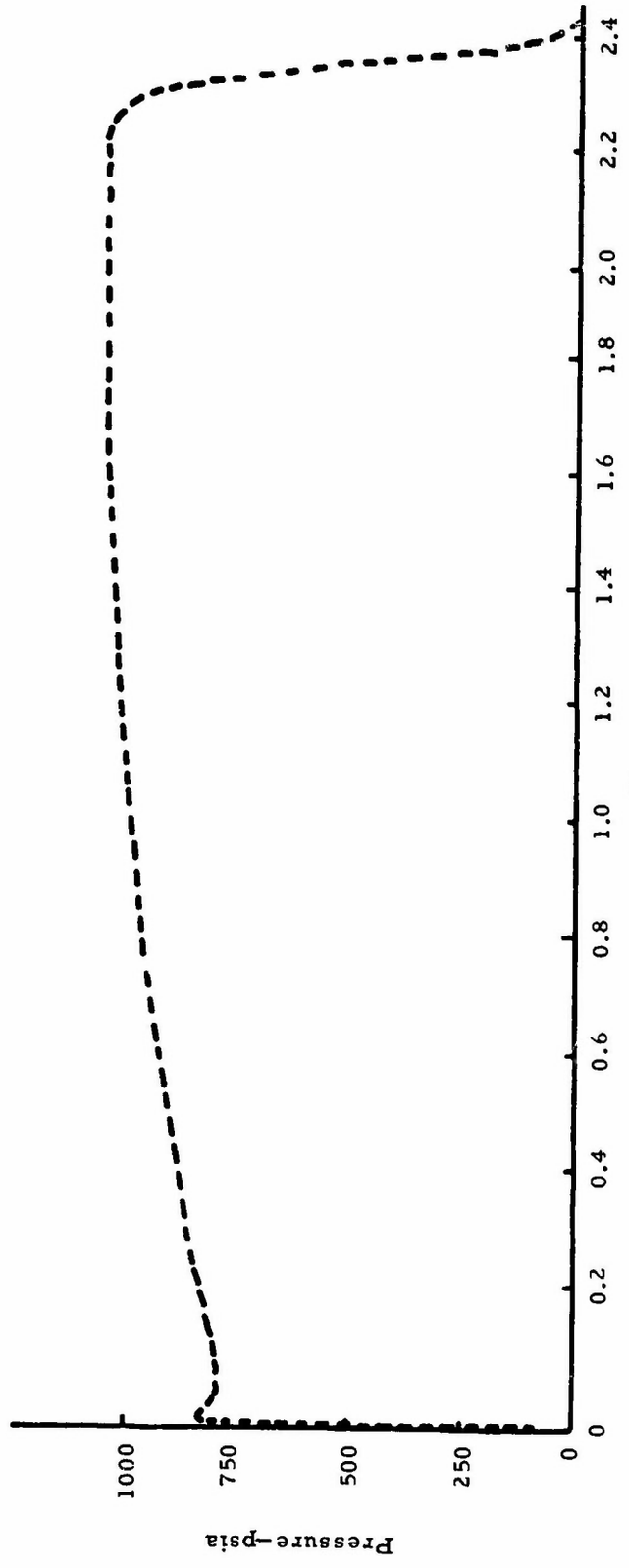

FIG. D-6 PRESSURE-TIME RECORD FROM 6CC18 FIRING.

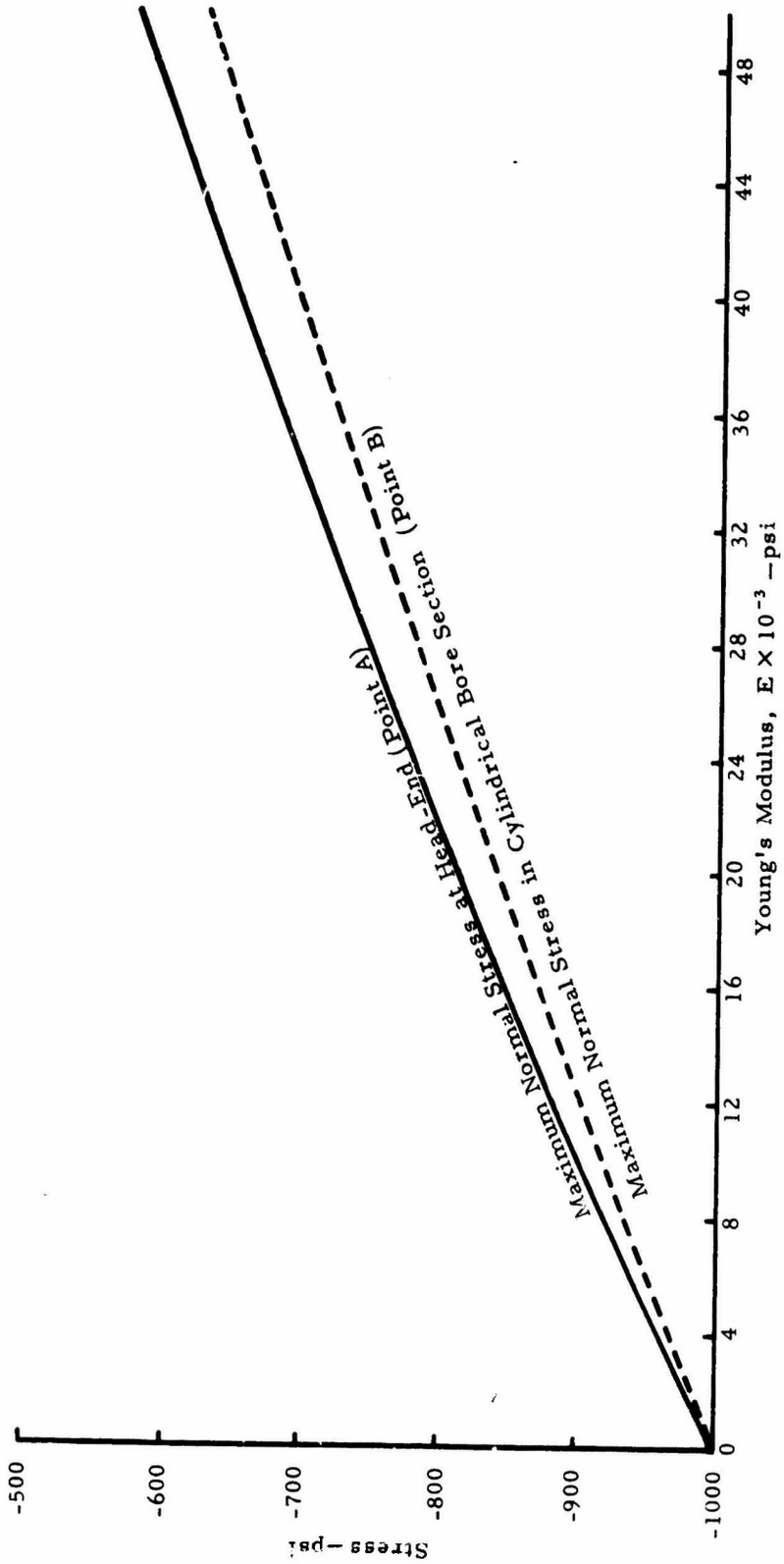

FIG. D-7 EFFECT OF YOUNG'S MODULUS ON MAXIMUM STRESS IN 6CC18 GRAIN DUE TO PRESSURIZATION.

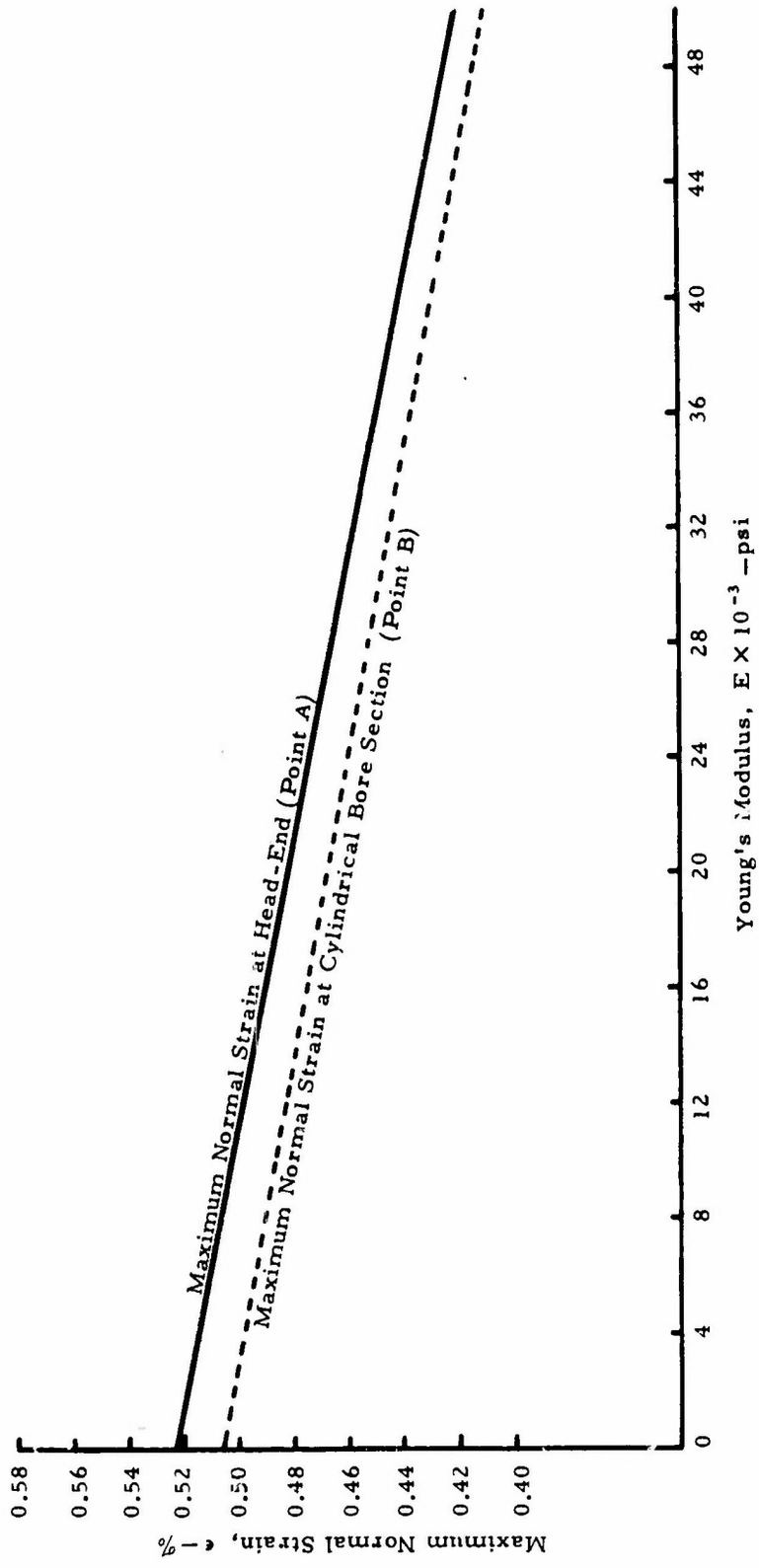

FIG. D-8 EFFECT OF YOUNG'S MODULUS ON MAXIMUM NORMAL STRAIN IN 6CC18 GRAIN DUE TO PRESSURIZATION.

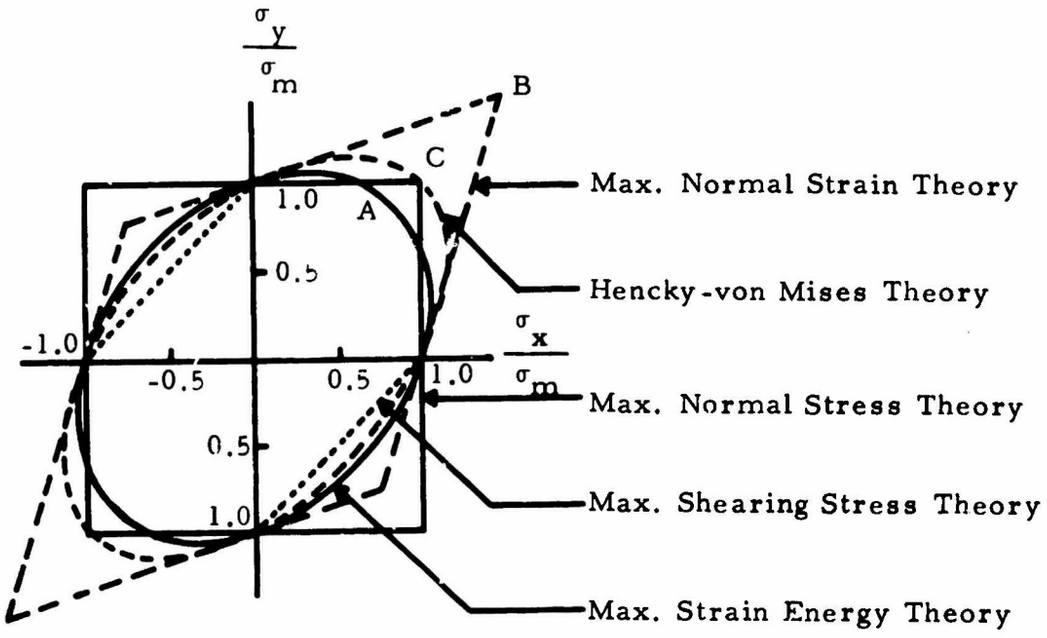

σ_x = Normal stress in x-direction.

σ_y = Normal stress in y-direction.

σ_m = Maximum allowable stress as determined in uniaxial test.

A = Biaxial failure stress less than uniaxial.

B = Biaxial failure stress greater than uniaxial.

C = Biaxial failure stress same as uniaxial.

FIG. D-9 FAILURE ENVELOPES FOR SEVERAL THEORIES OF FAILURE UNDER BIAXIAL STRESS CONDITIONS.

APPENDIX E

Structural Integrity of the Advanced Propellant Application Motor Loaded with Plastisol Nitrocellulose Propellant

Work done by: T. L. Cost

INTRODUCTION AND SUMMARY

An analysis was made of the structural integrity of the advanced propellant application motor assuming the motor loaded with a nitrocellulose plastisol propellant RH-P-112.[1] The loading conditions investigated were shrinkage resulting from curing at +120°F and cooling to -35°F and -65°F and pressurization resulting from ignition at +135°F, +78°F, -35°F, and -65°F. The experimental mechanical property data currently available on P-112 propellant do not adequately define the material mechanical behavior at low temperatures (-65°F) and high rates (30 in/in/min); however, estimates were made for these conditions. Although the data used were limited and possible errors exist due to extrapolations, results of the analysis indicate that the application motor loaded with P-112 propellant will withstand the shrinkage loads induced by cooling the motor to -35°F satisfactorily. The motor should also satisfactorily withstand the loads induced by ignition at +135°F, +78°F, and -35°F. However, results of the analysis indicate that cooling the motor to 65°F or ignition of the motor at -65°F will possibly result in failure. The structural integrity of the motor is marginal for these conditions. Due to the interest in the strength capabilities of the advanced propellants, a comparison was made of the predicted and allowable stresses and strains of SE-103A-1039 propellant with the corresponding quantities of the P-112-1270 plastisol propellant.

STRUCTURAL-INTEGRITY ANALYSIS

The configuration of the advanced propellant application motor analyzed is the 6CC18 design which is a completely axisymmetric body with a cross section as shown in Fig. E-1. The analysis performed on the application motor loaded with P-112 propellant utilized a portion of

[1] The mechanical property data used in the analysis were obtained by testing specimens from propellant batch P-112-1270.

the results obtained in the analysis of the application motor loaded with SE-103 propellant.[1] The geometry effects were determined in the analysis involving the SE-103 propellant and only the effect of different material properties and curing temperature needed to be taken into account in the analysis described here. The finite element method for elastic, axisymmetric, bodies was used in determining the geometry and material property effects for both analyses. The conditions examined included shrinkage from +120°F to -35°F and -65°F, and pressurization to 1000 psia in 10 msec at +135°F, +78°F, -35°F, and -65°F.

1. Mechanical Properties

All mechanical property data were obtained by the Applied Physics Group. Figs. E-2—E-5 illustrate the mechanical properties of the P-112 propellant. The modulus, maximum stress, strain at maximum stress, and shift factor at various temperatures are shown in these figures. The propellant was assumed to be elastic in dilation and a bulk modulus of 350,000 psi was used in the analysis. The volumetric coefficient of thermal expansion was obtained from SEC data to be 0.022%/°F. The case was assumed to be constructed of mild steel with a Young's modulus of 30×10^6 psi and a Poisson's ratio of 0.3. The case thickness used was 0.25 in.

The shift factor was determined from Fig. E-5 for the four temperatures of interest, as indicated previously, and the results are shown in Table E-I.

Table E-I

Shift Factor of RH-P-112 as a Function of Temperature

Temp. (°F)	$\log_{10}(a_T)$
+135	-0.85
+78	0
-35	+5.30
-65	+7.60

[1] Appendix B of this report.

2. Strain Rates

In general, the rate of loading of solid propellant materials influences both the predicted and allowable stresses and strains; hence, reasonable estimates must be made of this quantity.

a. Shrinkage - Based upon the results of the previous analysis, a calculation indicated that the application motor loaded with RH-P-112 propellant would experience a change in maximum normal strains of 0.0333%/°F. Cooling the motor from room temperature (78°F) to -65°F would result in a temperature change of 143°F and, hence, an applied strain of 4.59%. To be conservative, a strain of 5% was assumed applied in a cooldown time of 500 min. This assumption of the cooldown time is only an approximate estimate. An experimental measurement of this temperature variation would be needed for a better estimate due to the unknown boundary conditions surrounding the motor. The strain rate resulting from the above assumptions is

$$\dot{\epsilon} = \frac{0.05 \text{ in/in}}{500 \text{ min}} = 10^{-4} \frac{\text{in/in}}{\text{min}} .$$

This strain rate was assumed in analyzing the cooldown to -35°F also.

b. Pressurization - Experimental data presented in the analysis of the application motor with RH-SE-103 propellant indicated that the pressure would increase linearly from zero pressure and reach a maximum pressure of 1000 psia in 10 msec. Preliminary calculations indicated that the largest strain to be applied would be approximately 0.52%. The strain rate for pressurization thus becomes

$$\dot{\epsilon}_p = \frac{0.0052}{0.01} \frac{\text{in/in}}{\text{sec}} \cdot \frac{60 \text{ sec}}{\text{min}} = 31.2 \frac{\text{in/in}}{\text{min}} .$$

3. Reduced Times

For the strain rates calculated in Section 2 and the shift factor values presented in Table E-I, the reduced times for the shrinkage and pressurization loadings can be calculated and are presented in Table E-II. These reduced times allow the appropriate physical properties to be obtained from Figs. E-2 – E-4.

Table D-II

Reduced Times

Temp. (° F)	$\log_{10} \frac{1}{\dot{\epsilon}_s a_T}$	$\log_{10} \frac{1}{\dot{\epsilon}_p a_T}$
+135		-0.64
+78		-1.49
-35	-1.30	-6.79
-65	-3.60	-9.09

4. Predicted Stresses and Strains

The stress and strain values determined in the previous analysis as a function of modulus were used to predict the stresses and strains in the application motor loaded with RH-P-112 propellant.

a. Shrinkage - The RH-P-112 propellant was assumed to cure at +120° F and to experience a volumetric cure shrinkage of 0.5%.[1] This cure shrinkage results in a strain in the application motor of 2.25%. Calculations indicated that the maximum normal strain would occur approximately at point A in Fig. D-1. The magnitude of this strain due to temperature change is 0.0333%/° F. In addition, the linear thermal shrinkage term should be added to the actual strain to obtain the total strain from the unstressed state, the strain which is of interest in failure analyses. From these data, the predicted values of strain at -35° F and -65° F are shown in Table E-III.

Table E-III

Predicted Shrinkage Strains

	-35° F	-65° F
Strain due to cure shrinkage	= 2.25%	= 2.25%
Strain due to thermal shrinkage load	(0.0333)(155) = 5.16%	(0.0333)(185) = 6.16%
Strain due to thermal shrinkage	(0.00734)(155) = 1.14%	(0.00734)(185) = 1.36%
Total strain from unstressed state	8.55%	9.77%

[1]This value obtained from SEC data.

b. Pressurization - The stresses and strains in the application motor are functions of modulus for pressurization loadings. The modulus value of the propellant depends upon the temperatures and strain rates. The modulus values for the temperatures and pressurization strain rates which correspond to the reduced times in Table E-II can be determined from Fig. E-2. These values are presented in Table E-IV.

Table E-IV

Tangent Modulus

Temp. (°F)	E (psi)
+135	645
+78	1,000
-35	12,300
-65	36,300

The variation of the maximum stress and strain which occurs at point A, Fig. E-1, with modulus is presented in Figs. E-6 and E-7. From these figures the maximum predicted stresses and strains corresponding to the modulus values in Table E-IV can be obtained. The results are shown in Table E-V. The stresses in Table E-V ignore the 1000 psi hydrostatic compressive stress due to the chamber pressure.

Table E-V

Predicted Stresses and Strains for Pressurization

Temp. (°F)	Stress (psi)	Strain (%)
+135	6	0.521
+78	8	0.520
-35	120	0.498
-65	321	0.448

5. Allowable Stresses and Strains

Although the stress and strain fields present in an actual motor are multiaxial, the only high-rate failure data available at these Laboratories are obtained from uniaxial tensile tests. Due to this

difference, the uniaxial data should not be applied directly in predicting failure in multiaxial stress fields. However, the uniaxial data can be modified approximately to make them applicable. The uniaxial failure limits for RH-P-112 propellant can be obtained from Figs. E-3 and E-4 for the reduced times presented in Table E-II. The allowable stresses and strains for the shrinkage and pressurization loadings are presented in Tables E-VI and E-VII, respectively.

Table E-VI

Allowable Uniaxial Strains for Shrinkage Loading

Temp. (°F)	Strain (%)
-35	17.3
-65	15.3

Table E-VII

Allowable Uniaxial Stresses and Strains for Pressurization Loading

Temp. (°F)	Stress (psi)	Strain (%)
+135	77.6	17.60
+78	109.5	17.30
-35	976.0	8.10
-65	2510.0	0.78

DISCUSSION OF RESULTS

Since the uniaxial failure data presented in Tables E-VI and E-VII are not directly applicable to the actual multiaxial condition in the motor, the uniaxial data must be modified. Based upon the arguments presented in the previous analysis of the application motor, the allowable strains from the uniaxial tests should be multiplied by approximately 67% and the allowable stresses by 80%. After these reductions were made, a comparison was made between the predicted and allowable values. These comparisons are presented in Tables E-VIII and E-IX. The predicted values were obtained from Tables E-III and E-V.

Table E-VIII

Comparison of Predicted and Allowable Strains for Shrinkage Loading (RH-P-112-1270)

Temp. (°F)	Strain[a] (%/%)
-35	8.55/11.59
-65	9.77/10.03

[a]Predicted/allowable

Table E-IX

Comparison of Predicted and Allowable Stresses and Strains for Pressurization Loading (RH-P-112-1270)

Temp. (°F)	Stress[a] (psi/psi)	Strain[a] (%/%)
+135	6/62	0.521/11.80
+78	8/87	0.520/11.60
-35	120/781	0.498/5.43
-65	321/2005	0.448/0.52

[a]Predicted/allowable

By inspection of Tables E-VIII and E-IX it appears that there are two conditions which are marginal from a structural integrity standpoint: shrinkage to -65°F and pressurization at -65°F. Although the margins of safety for both conditions are slightly positive, the difference between the predicted and allowable strains is small enough to warrant concern.

There are many limitations upon the comparisons presented in Tables E-VIII and E-IX. Several of these limitations have been discussed previously; however, it should be recognized that effects such as ablation due to burning, cumulative damage effects, superposed hydrostatic pressure on tensile tests results and other factors have not been taken into account in this analysis.

Since the strength characteristics of the advanced propellants under development at these Laboratories are of interest, it appears appropriate to compare the strength characteristics of plastisol RH-P-112-1270 propellant with those of an advanced propellant such as RH-SE-103A-1039 under the same conditions. The RH-SE-103A-1039 propellant was investigated in the analysis described previously and the results of that analysis are included in Tables E-X and E-XI for comparative purposes. It should be recalled that the low temperature (-65°F), high-rate (30 in/in/min) data for the RH-SE-103A-1039 propellant were inadequate and had to be extrapolated to these conditions. This was also true of the RH-P-112-1270 propellant.

Table E-X

Comparison of Predicted and Allowable Strains for Shrinkage Loading

Temp. (°F)	Strain[a] (%/%) (RH-P-112-1270)	Strain[a] (%/%) (RH-SE-103-1039)
-35	8.55/11.58	7.42/20.0
-65	9.77/10.03	8.52/14.6

[a]Predicted/allowable.

Table E-XI

Comparison of Predicted and Allowable Stresses and Strains for Pressurization Loading

	RH-P-112-1270		RH-SE-103-1039	
Temp. (°F)	Stress[a] (psi/psi)	Strain[a] (%/%)	Stress[a] (psi/psi)	Strain[a] (%/%)
+135	6/62	0.521/11.80	6/38.4	0.542/19.3
+78	8/87	0.520/11.60	8/59.1	0.542/20.6
-35	120/781	0.498/5.43	44/333	0.534/10.6
-65	321/2005	0.448/0.52	561/746	0.407/0.670

[a]Predicted/allowable.

CONCLUSIONS

Based upon the results of the analysis the following conclusions may be drawn:

(1) The application motor loaded with RH-P-112 propellant should satisfactorily withstand the shrinkage induced by cooling to -35°F.

(2) The application motor loaded with RH-P-112 propellant should satisfactorily withstand ignition at +135°F, +78°F, and -35°F.

(3) The conditions associated with shrinkage to -65°F and ignition at -65°F in the application motor filled with RH-P-112 propellant produce a motor with only marginal structural integrity. The strain ratios presented in Tables E-VIII and E-IX for this propellant and for these conditions could very easily be reversed in reality.

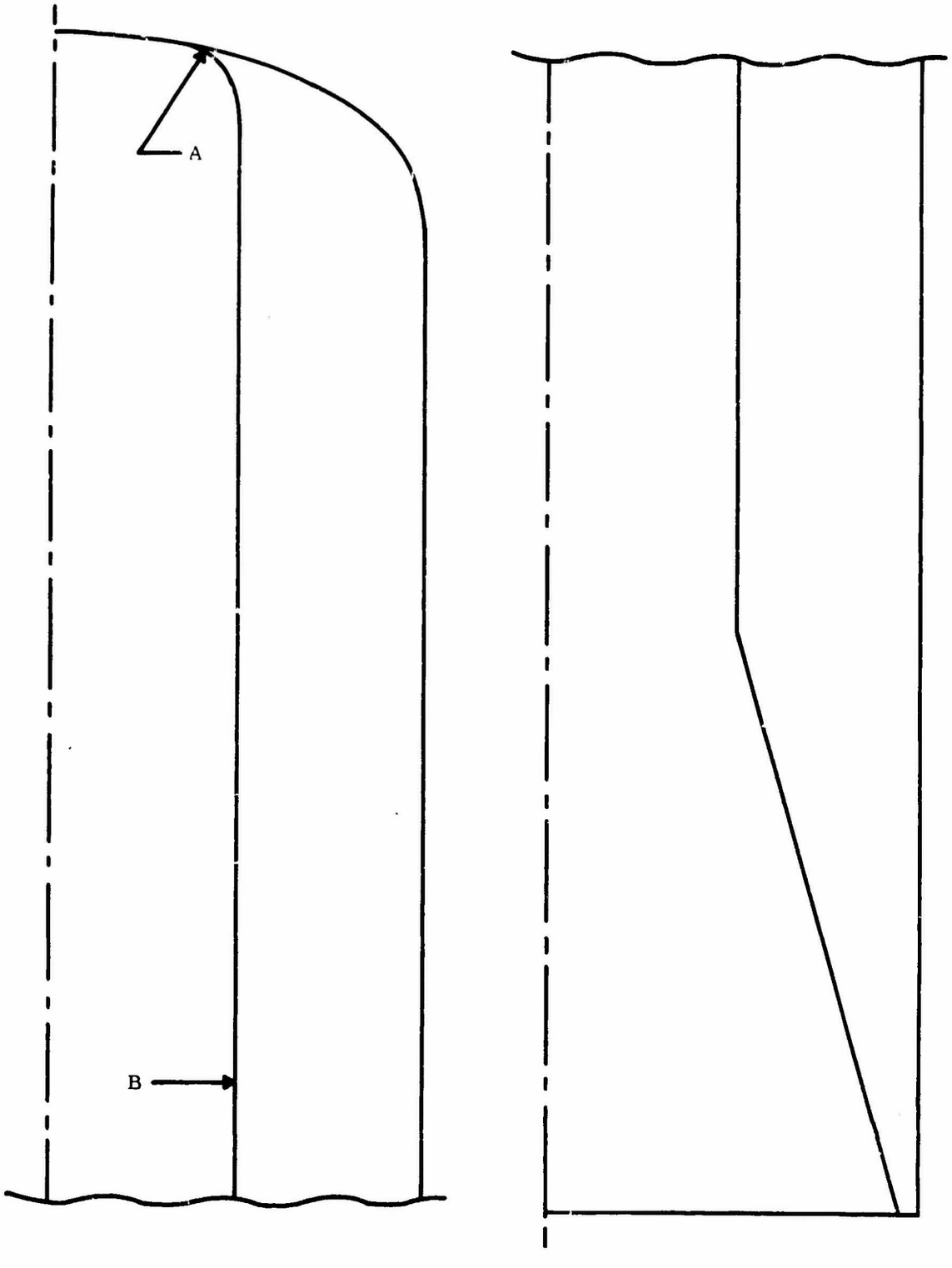

FIG. E-1 CROSS-SECTION OF 6CC18 APPLICATION MOTOR GRAIN WITH STRESS-RELIEF FILLET; LENGTH = 18 in., O.D. = 6 in., I.D. = 3 in.

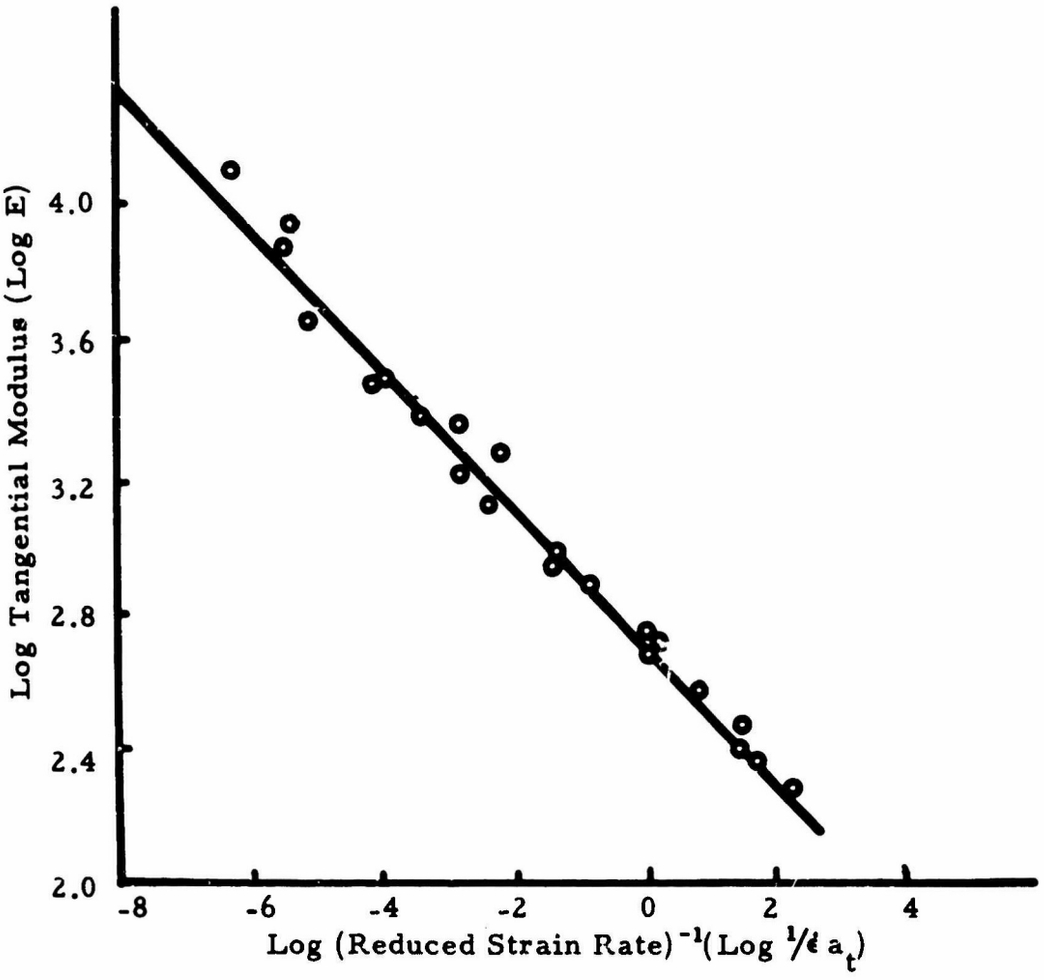

FIG. E-2 TANGENT MODULUS VERSUS REDUCED STRAIN RATE FOR RH-P-112 PROPELLANT.

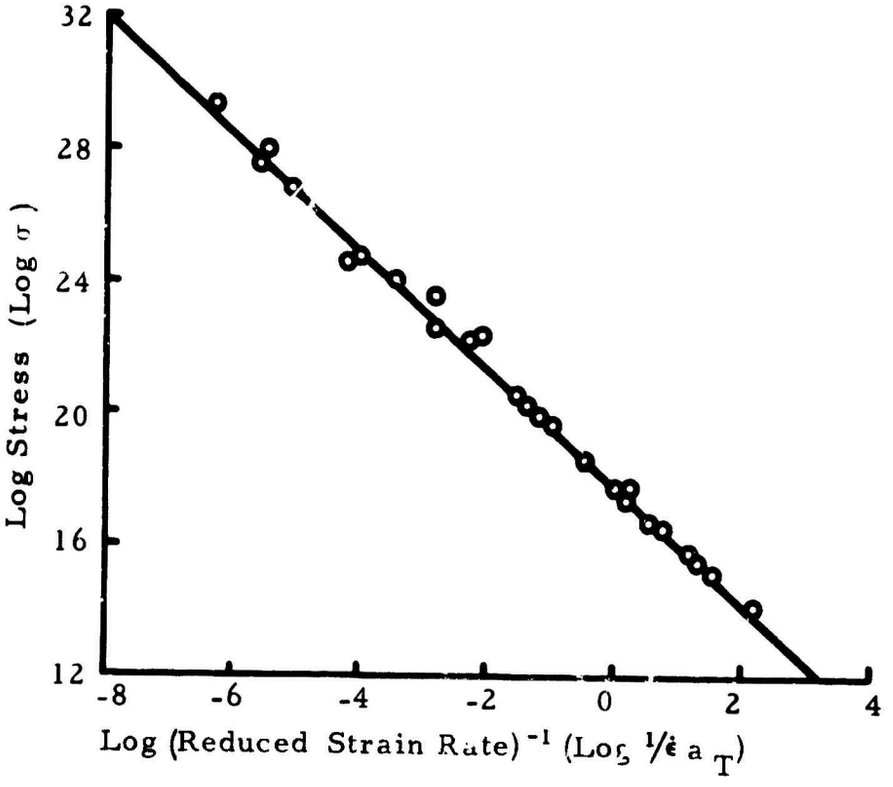

FIG. E-3 MAXIMUM STRESS VERSUS REDUCED STRAIN RATE FOR RH-P-112 PROPELLANT.

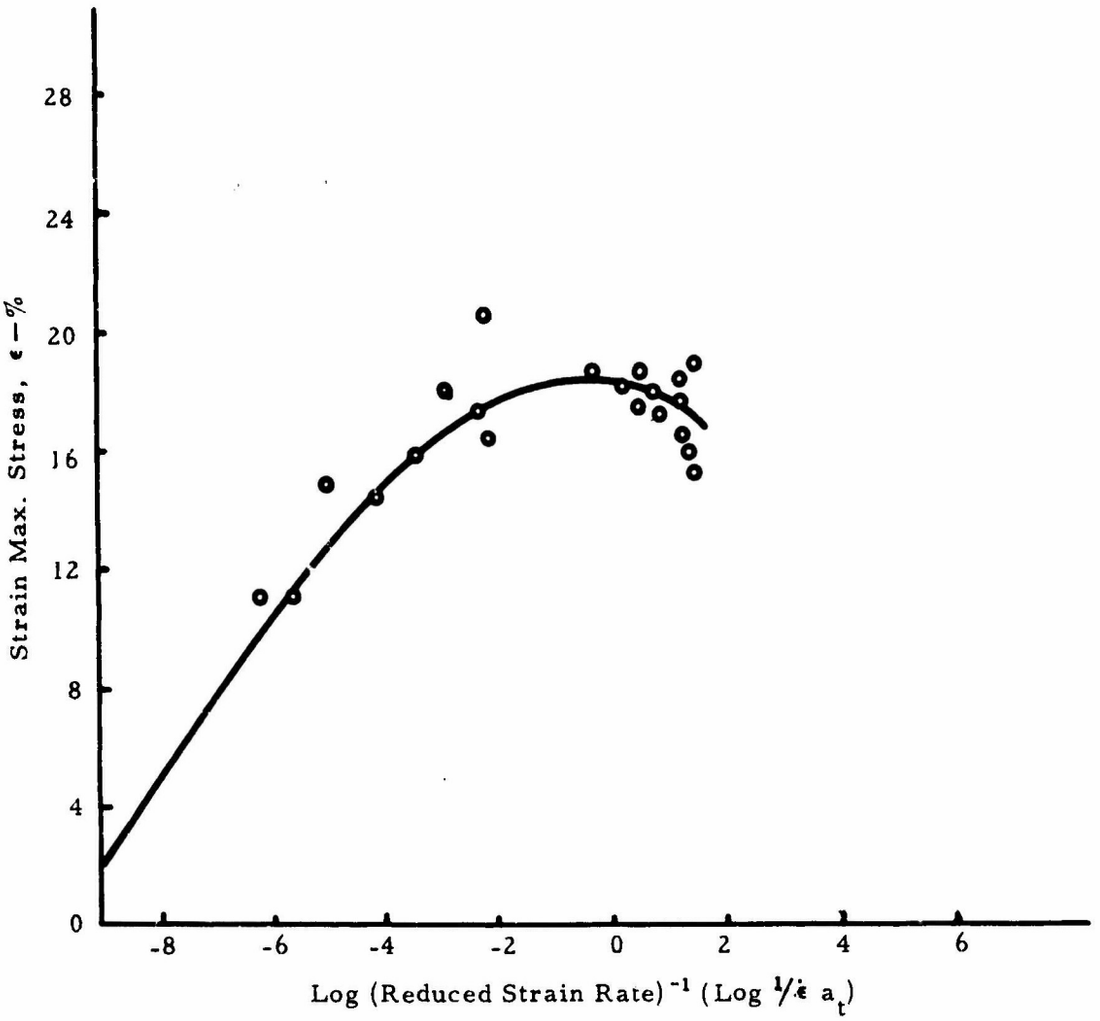

FIG. E-4 STRAIN AT MAXIMUM STRESS VERSUS REDUCED STRAIN RATE FOR RH-P-1!2 PROPELLANT.

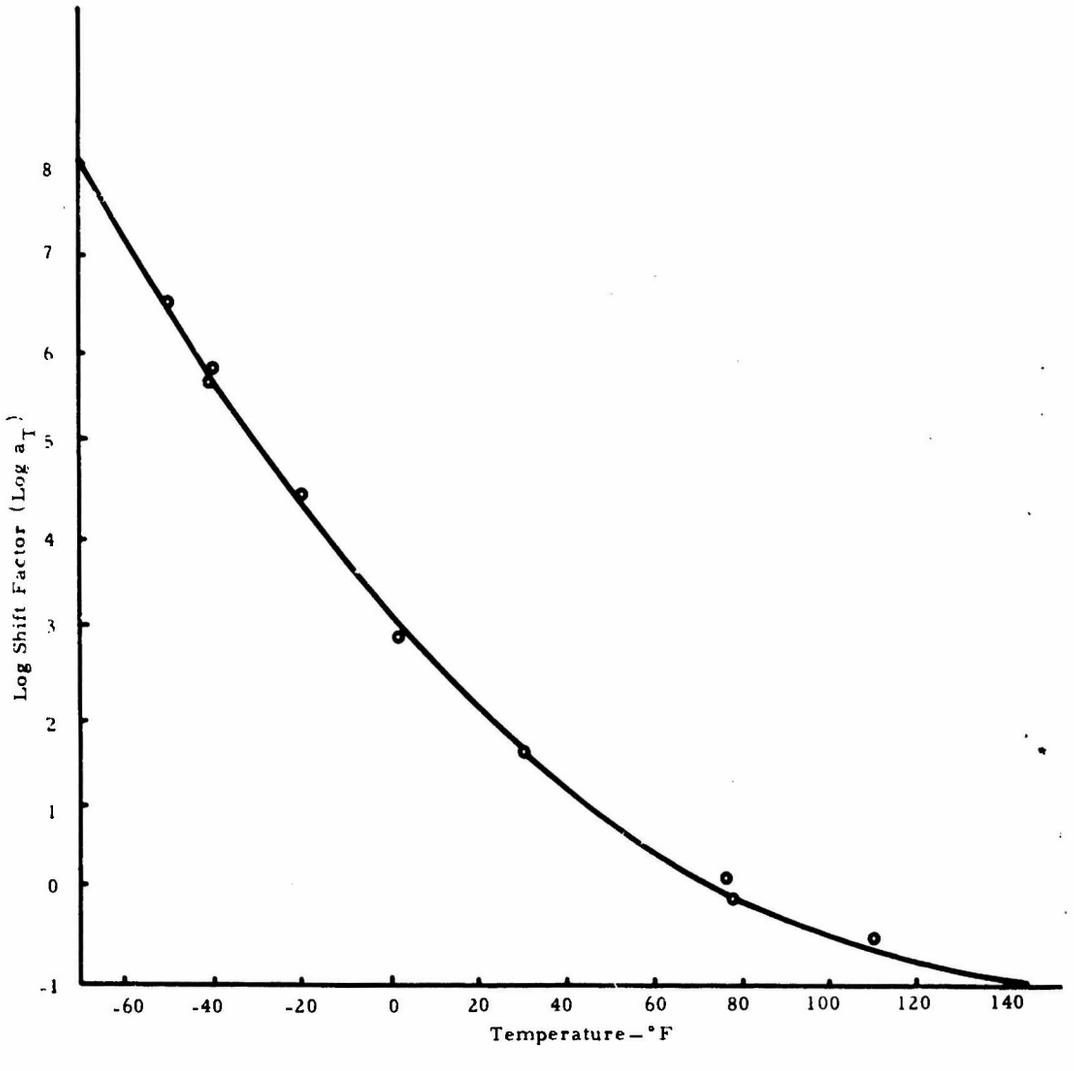

FIG. E-5 SHIFT FACTOR VERSUS TEMPERATURE FOR RH-P-112 PROPELLANT.

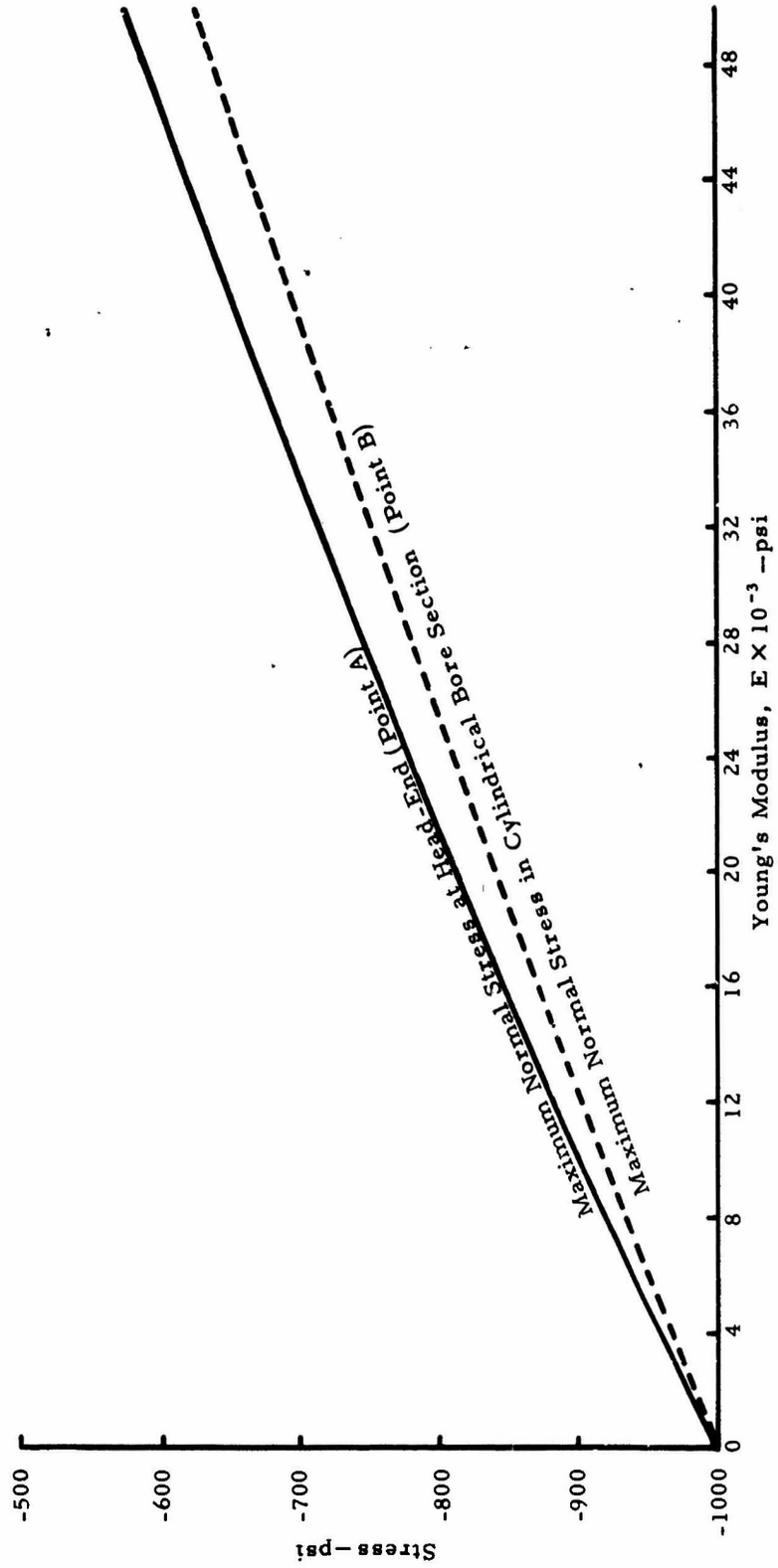

FIG. E-6 EFFECT OF YOUNG'S MODULUS ON MAXIMUM STRESS IN 6CC18 GRAIN DUE TO PRESSURIZATION.

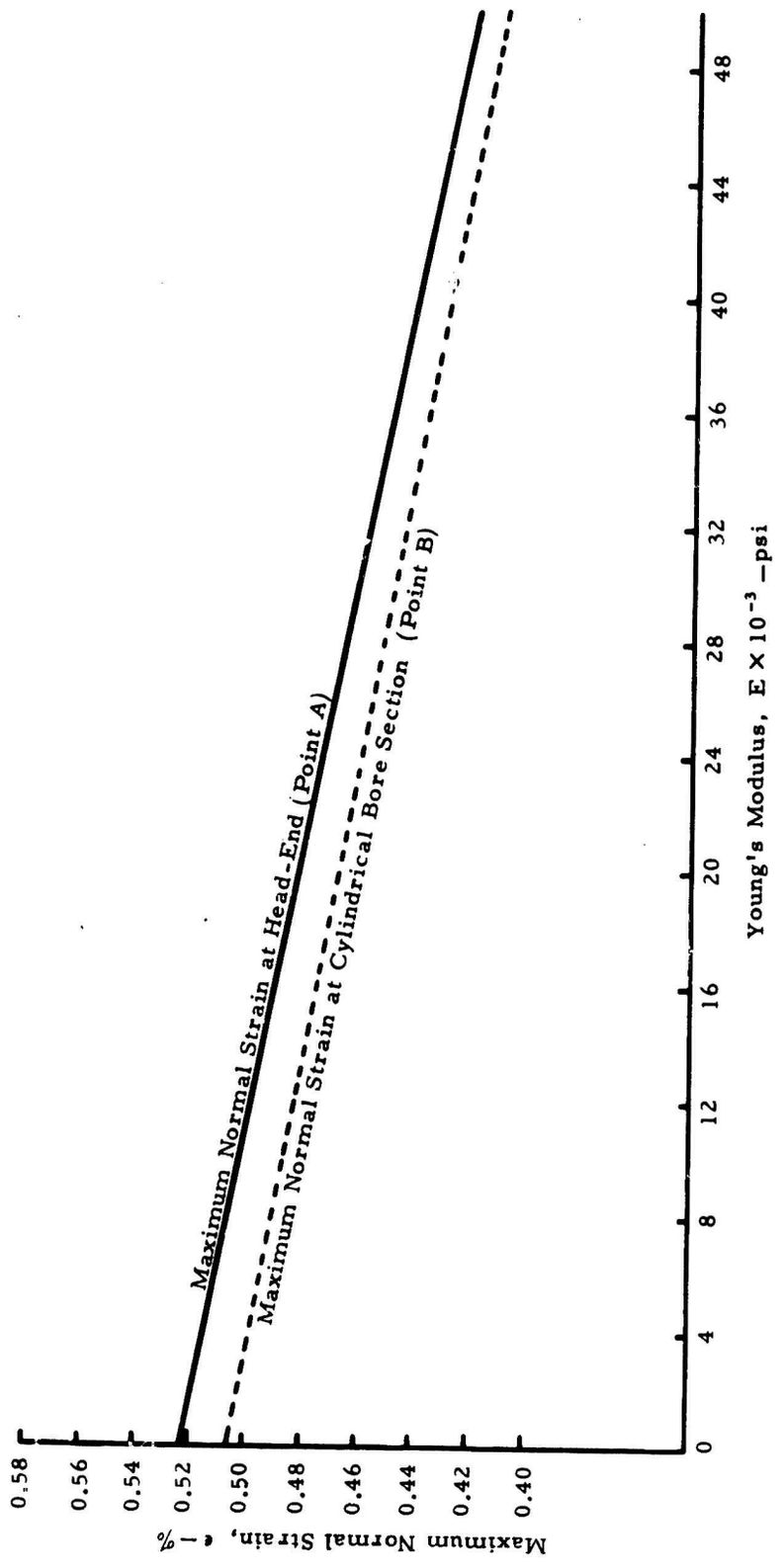

FIG. E-7 EFFECT OF YOUNG'S MODULUS ON MAXIMUM NORMAL STRAIN IN 6CC18 GRAIN DUE TO PRESSURIZATION.

APPENDIX F

High-Rate Hydrotest Technique

A test to verify the structural integrity of the 6CC18 motor under ignition loads was necessary. The only practicable method seemed to be to use a hydrostatic medium pressurized by gas. Entirely pneumatic pressurization would require moving a large volume of gas (enough to pressurize the free volume of the motor to 1000 psia) in less than 10 milliseconds. By filling the motor free volume with liquid, the volume of gas necessary was reduced drastically and reasonable orifice sizes could be used to obtain a short pressure-rise time. The arrangement used is shown schematically in Fig. F-1.

The most significant problem was obtaining a fluid which would not freeze at -65°F, and which would not absorb or react with propellant ingredients. Dow-Corning 200 silicone fluid fulfilled these requirements. Infra-red analyses showed that fluid in which propellant had been soaked absorbed no propellant ingredients, and the soaked propellant was not softened or attacked by the fluid. The fluid viscosity remained low at temperatures well below those required.

Plumbing and free volume were tested using a water-filled motor at ambient temperature. The MV-121[1] valve provided more than adequate gas flow area for the volume used. Pressure-rise rates were different at the head and tail (indicating the time taken for the pressure wave to traverse the length of the motor) but were still higher than those experienced during a typical ignition (this illustration is shown in Fig. 5 in the body of the report). Control over the rise time is available by simply varying the height of the liquid in the tube between the valve and the motor (Fig. F-1).

A second test was run with a live motor at -35°F. Again, no problems with the system were encountered and a pressure of 990 psia was reached in 10 milliseconds. This motor was drained, dried, reconditioned, and fired successfully at -35°F.

[1]Marotta Valve Corp., Boonton, New Jersey.

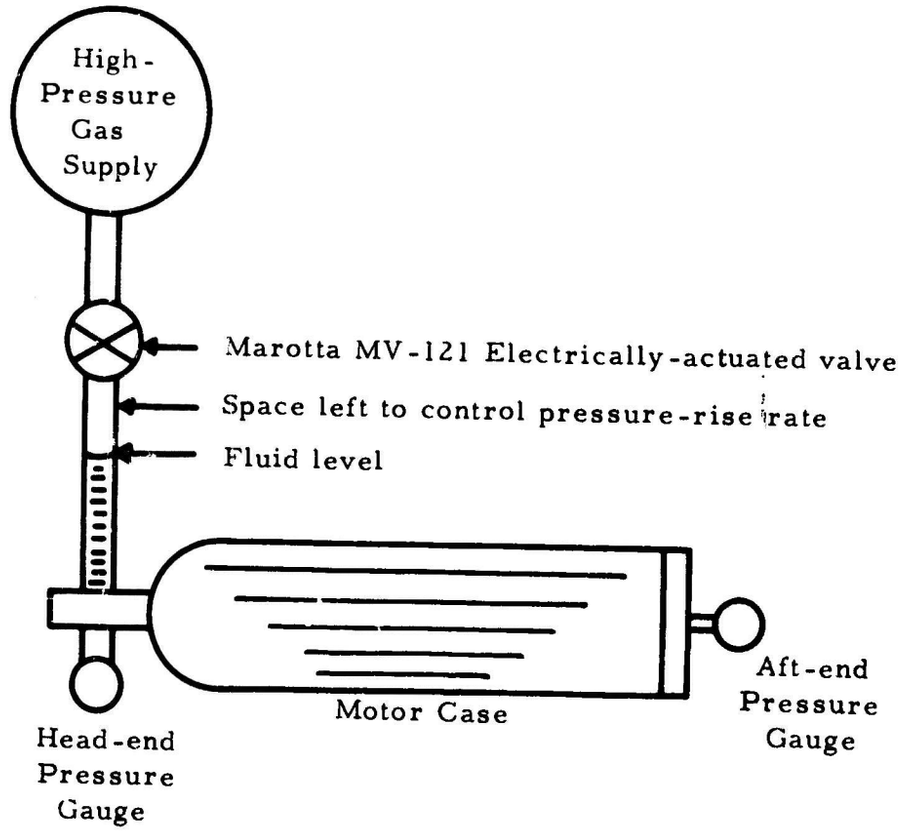

FIG. F-1 SCHEMATIC OF HIGH-RATE HYDROSTATIC TEST SYSTEM.

Initial distribution of this report has been made in accordance with "Chemical Propulsion Mailing List", CPIA Publication 74, March 1965 and approved supplements.

Qualified users may obtain this report from the Defense Documentation Center.

In addition to security requirements which must be met, this document is subject to special export controls, and each transmittal to foreign governments or foreign nationals may be made only with prior approval of

Department of Army
Headquarters, U. S. Army Missile Command
Redstone Arsenal, Alabama 35809